Site Amplification at Permanent Stations in Northeastern Italy

Peter Klin[*1] , Giovanna Laurenzano[1] , Carla Barnaba[1] , Enrico Priolo[1] , and Stefano Parolai[1]

ABSTRACT

The application of earthquake recordings to the estimation of an event's magnitude and the construction of rapid-response ground-motion maps requires an adequate classification of the recording stations in terms of their site response. For permanent stations, this information can be obtained from a sufficiently large database of past recordings.In this work, we analyze more than 7300 three-component recordings collected between 1996 and 2017 by 67 permanent stations in northeastern Italy to assess their site amplification. The signals come from 368 earthquakes with a magnitude range of M 3.2–5.8 and a distance range of 10–300 km. We evaluate the frequency-dependent amplification function with respect to a reference station with a flat seismic noise horizontal-to-vertical spectral ratio. The evaluation relies on the decomposition of the S-wave amplitude spectra in terms of source, propagation, and site response. We solve the decomposition with a nonparametric, single-step generalized inversion in the frequency band 0.5–20 Hz. In addition, we compute the amplification factors for peak ground acceleration and velocity with respect to a well-established ground-motion prediction equation. The results highlight that only 11 stations show a relatively flat unitary response with respect to the reference site, whereas the frequency-averaged amplification function at 23 out of 67 stations exhibits a value larger than 2. We classified the sites according to their surface geology and geomorphological scenario and found that amplification affects not only stations installed on the alluvial soil but also several stations installed on what are assumed to be rock sites. Sites in caves and mines exhibit deamplification, whereas the stations with sensors in boreholes exhibit the typical interference pattern. A good correlation between the amplification factors and the frequency-averaged amplification functions suggests the possibility of predicting time-domain peak ground-motion values from amplification functions estimated by generalized inversion.
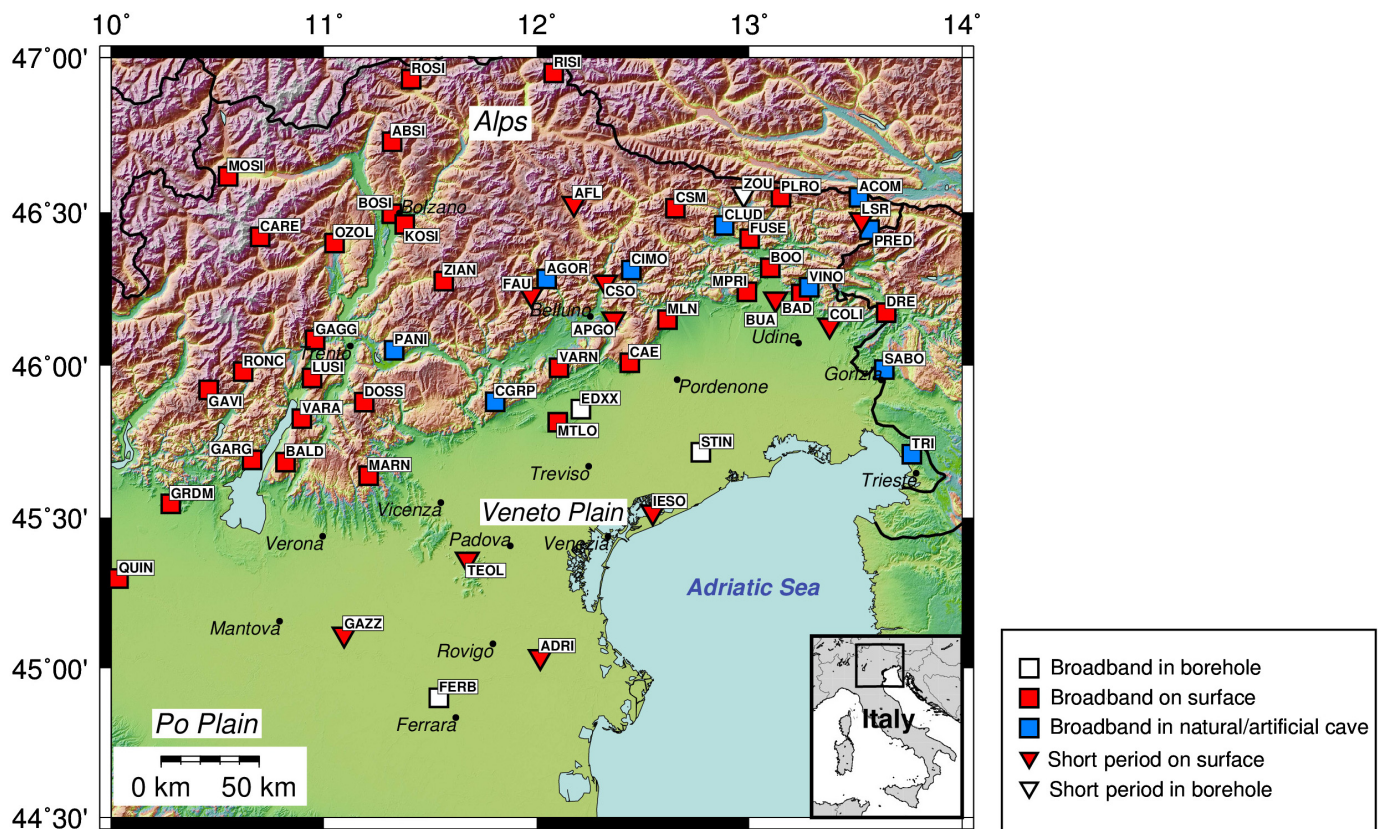
KEY POINTS

- We evaluate the site amplification at 67 permanent seismic stations in Northeastern Italy.
- At several stations, the site effects significantly influence the PGV, PGA, and frequency response.
- The evaluated site amplification properties may improve the usage of seismic recordings from these stations.

Supplemental Material

INTRODUCTION

In northeastern Italy, the deformed northern margin of the Adria microplate interacts with three orogenic belts, namely, the Alpine chain in the north, the External Dinarides in the east, and the Northern Apennines in the south (Castellarin *et al.*, 2006). This complex setting implies the occurrence of moderate-to-strong earthquakes; according to the Parametric Catalogue of Italian Earthquakes (CPTI15) (Rovida *et al.*, 2020), 14 earthquakes with a magnitude greater than M_w 6 have struck this area over the last 1000 yr. A large portion of the densely populated zones of northeastern Italy, however, has only required seismic regulations since 2003 (Stucchi *et al.*, 2011), and the combination of seismic hazard and inadequate seismic design potentially leads to high levels of seismic risk. Nevertheless, a reliable assessment of seismic hazard in the study area requires an accurate characterization of the possible seismic sources, the attenuation of the seismic waves from their source to the investigated site, and the effects of the shallow local geology on ground motion, that is, site amplification. This information is essential

Figure 1. The 67 permanent stations considered in the present study have different instrumentation (broadband or short period) and are located in sites with different typologies. The label EDXX indicates the location of the Collalto Seismic Network, which consists of 10 stations (ED01–ED10). The inset in the map shows the location of the study area. The color version of this figure is available only in the electronic edition.

also in the computation of rapid-response ground-motion maps (Wald *et al.*, 1999) and in rapid damage scenario assessment for earthquake emergency management (Poggi *et al.*, 2021).

The awareness of the seismic risk in northeastern Italy has fostered the deployment of an ever-growing number of permanent stations devoted to seismic monitoring and emergency management purposes (Priolo *et al.*, 2005; Bragato *et al.*, 2021). The National Institute of Oceanography and Applied Geophysics (OGS) manages the Northeast Italy Seismic Network (NEI), which consists of about 40 stations and covers the entire Friuli-Venezia Giulia and Veneto Regions as well as marginal parts of Lombardia and Emilia-Romagna. Furthermore, 16 permanent stations in the Trentino-Alto Adige-Südtirol region enter the NEI system within the framework of collaboration agreements between the OGS and local civil protection institutions. All of these instruments make possible an exhaustive coverage of northeastern Italy over an area of about 400 × 300 km (Fig. 1). In addition to NEI, OGS manages the Collalto Seismic Network, a local network with the aim of monitoring the seismicity in an area near the underground gas storage site of Montello-Collalto, located at the northern margin of the Venetian Plain. This network consists of 10 broadband seismological stations, all of which are equipped with borehole or posthole seismometers (Priolo *et al.*, 2014). In total, almost 70 permanent stations in northeastern Italy provide seismic recordings in real time, as of 2021. The location of these stations ranges from the top of alpine mountains to the alluvial plain of the Po

River (Fig. 1). As is well known, topography and/or inhomogeneous distribution of material properties near the Earth's surface at the station's site produce modifications of seismic motion that are usually referred to as site response (Boore, 2004). Site response can affect recordings of earthquakes (e.g., Tucker *et al.*, 1984; Chen and Wang, 2018), and a characterization of the site conditions (e.g., Drouet *et al.*, 2010; Michel *et al.*, 2014) should be a prerequisite for the correct usage of the recordings. Applications for seismic hazard assessment, such as the derivation of intensity prediction equations (Panzera *et al.*, 2020), also rely on the identification of the site response at the seismic stations of a regional network.

However, only a limited subset of the stations in northeastern Italy, mainly located in the Friuli-Venezia Giulia area, have been involved in site-response studies thus far. Malagnini *et al.* (2004) showed how stations on rock sites in the area might exhibit nonflat responses due to shallow heterogeneities resulting from varying degrees of weathering. In their attempt to reduce the uncertainty associated with ground-motion relations, Bragato and Slejko (2005) found that

average station residuals at several permanent stations are not correlated with the soil class that was assigned following the criteria in Ambraseys *et al.* (1996). On the other hand, Bragato and Slejko (2005) found a good correlation between station peak horizontal acceleration residuals and the average in the 1–8 Hz frequency band of the horizontal-to-vertical spectral ratio of earthquake recordings. The horizontal-to-vertical spectral ratio of earthquake recordings is a popular proxy for site response (Lermo and Chávez-García, 1993), and in the present work we denote it as EHV. Franceschina *et al.* (2013) found it necessary to consider EHV at some stations in Friuli to reduce misfits in earthquake source characterization studies and evidenced the need for an adequate description of the site response at the recording stations. Even though the cited studies have considered only stations deployed in the Friuli area, we can reasonably expect nonflat site responses also at the permanent stations in the remaining part of northeastern Italy, especially for the stations located in the Po Valley (Fig. 1). In fact, stations in the Po Valley can exhibit strong amplification peaks at low as well as high frequencies (Massa *et al.*, 2017) because they are necessarily deployed on thick layers of soft Quaternary sediments that hide a quite complex geological setting (Klin *et al.*, 2019). Moratto *et al.* (2019) estimated nonflat seismic response for the 10 seismological stations of the Collalto Seismic Network (which are part of this study) using one nearby NEI station as a reference.

The cited studies expose the need for an accurate definition of the site response at the permanent stations in northeastern Italy. A clear advancement with respect to the available knowledge is possible because over the past two decades the permanent stations in northeastern Italy have acquired recordings that correspond to hundreds of moderate (M >3.2) events. These recordings constitute a sufficiently large database to perform a comprehensive study of the weak-motion site response at these stations. In this study, we focus on the evaluation of site amplification at the permanent stations managed by OGS and at the other permanent stations that were active in northeastern Italy during the period 1996–2017.

Among the available approaches for site-response estimation (e.g., Parolai, 2012), in the present work we adopt the one-step nonparametric generalized inversion technique (GIT; Oth *et al.*, 2011), which allows for the evaluation of the site response in terms of the expected Fourier amplitude spectra (FAS) amplification with respect to a predefined reference site. To help the identification of reference sites when their site classification is not available, a number of selection criteria based on waveform data analysis (i.e., seismological proxies) have been proposed (e.g., Parolai *et al.*, 2004; Priolo *et al.*, 2020). To this regard, in addition to the GIT inversion, we consider the analysis of the seismic noise horizontal-to-vertical spectral ratio (NHV; Nakamura, 1989) and the abovementioned EHV (Lermo and Chávez-García, 1993). We introduce quantitative criteria that allows for classifying the evaluated site

amplification functions within five categories, whereas the 67 sites are grouped into 11 geomorphological scenarios (Biolchi *et al.*, 2011) and 13 types of surface geology. Finally, we estimate the site effects in terms of peak ground velocity (PGV) and peak ground acceleration (PGA) interevent amplification factors by considering as reference the ground-motion prediction equation (GMPE) of Bindi *et al.* (2011) for Eurocode 8 soil class A (Eurocode 8, 2004).
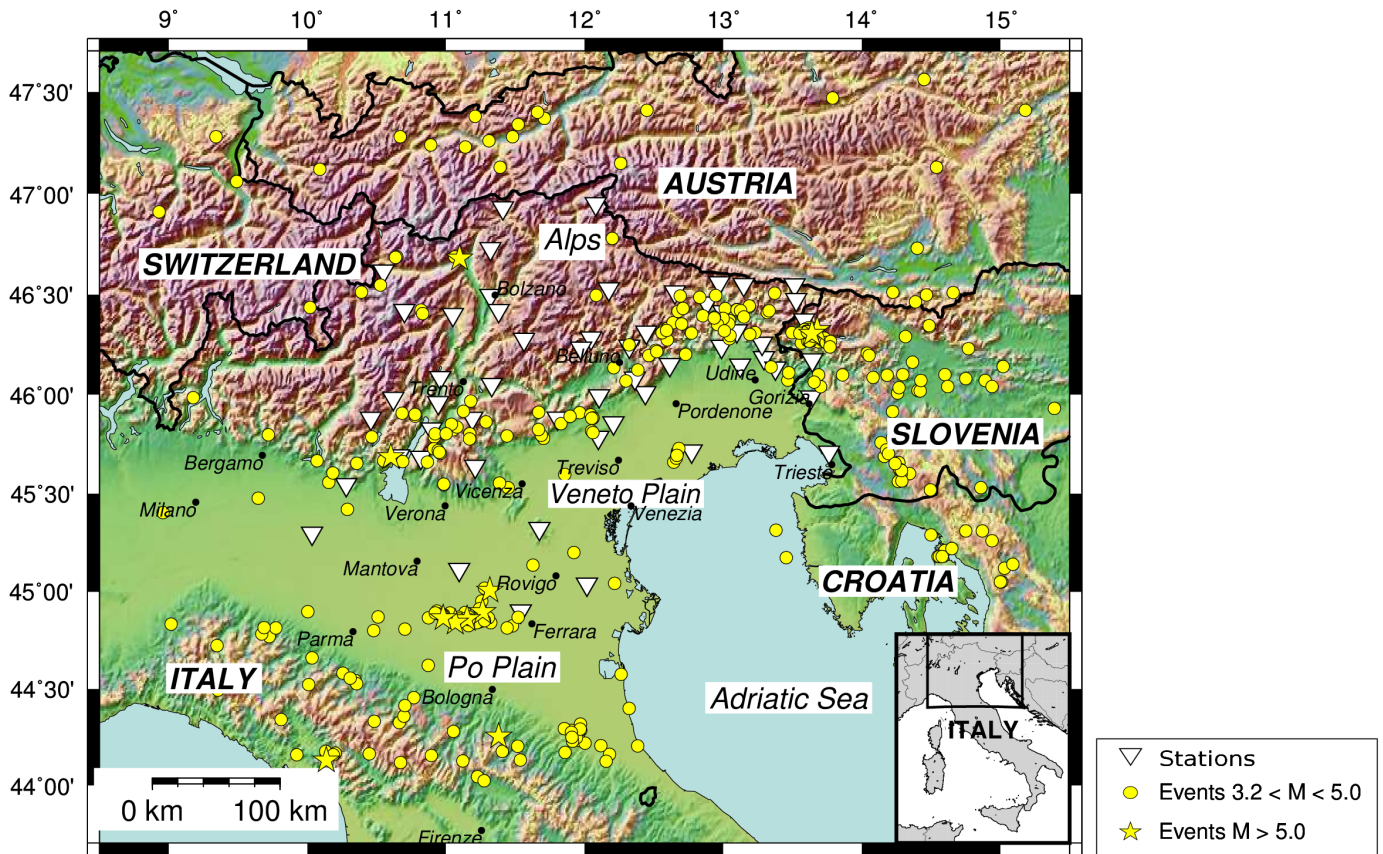
STATIONS AND DATA

The data employed in this study consist of recordings of events with a magnitude greater than M 3.2 collected between 1996 and 2017 at permanent stations installed in northeastern Italy. A higher magnitude threshold (M >3.5) was set for the events belonging to the 2012 Emilia-Romagna sequence to avoid an overweighting contribution of data from this area. The final dataset consists of 368 events having epicentral distances shorter than 300 km and recorded by at least two permanent stations considered in this work (Fig. 2). We based our search on the bulletin of the OGS Seismological Research Centre (OGS, n.d.), on the Italian Seismological Instrumental and Parametric Data-Base (ISIDe; ISIDe Working Group, 2007), and on the Euro-Med Bulletin catalog of the European-Mediterranean Seismological Centre (EMSC, n.d.).

The magnitude distribution plots concerning the selected events are given in Figure 3. The strongest events included in our database are the 12 April 1998 M 5.8 event in Slovenia and the 20 and 29 May 2012 events in Emilia-Romagna (Italy) with magnitudes of M_L 5.8 and M_L 5.6, respectively. The hypocentral depth of the events in the database does not exceed 35 km, with two outliers with depths of around 70 km located southwest of the investigated area, under the Northern Apennines (see Fig. 2).

We extracted the recordings corresponding to the 368 events from the OGS Archive System of Instrumental Seismology (OASIS; Priolo *et al.*, 2015) and corrected them for instrumental response. We discarded the recordings that featured an average signal-to-noise ratio of less than 10 or that were affected by spikes, saturation, or overlapping of events in a seismic sequence. In the analysis, only the stations that correctly recorded more than 10 of the identified events were considered. The three-component recordings were used.

The 67 permanent stations employed in this study are listed in Table 1, and their locations are shown in Figure 1. Almost all stations have sensors deployed on the surface. The exceptions are as follows:

- ACOM, CGRP, CIMO, PANI, and SABO in dismissed military bunkers.
- FERB in a 130-meter-deep borehole.
- PRED, CLUD, and AGOR in former mines.
- Stations of the Collalto network (ED01–ED10) in boreholes at depths ranging from 13 to 151 m.

Figure 2. We considered the recordings of 368 seismic events between 1996 and 2017 with magnitudes M >3.2 and with epicentral distances of less than 300 km from at least two of the stations. The distribution of epicenters marks the main seismically active areas that affect the seismic hazard in northeastern Italy: the fore-Alps in Veneto and Friuli, the western Dinarides (including their junction with the Alps), and the Northern Apennines (including those buried under the Po Plain). The inset in the map shows the location of the study area. The color version of this figure is available only in the electronic edition.

- STIN equipped with two sensors, STI0 at the surface and STI1 in a 100-meter-deep borehole.
- TRI and VINO in natural caves.
- ZOU2 in a 10-meter-deep borehole.
- BALD and TEOL in a masonry hut.

During the considered study period, the networks underwent several changes; therefore, the dataset is not homogeneous. As can be understood from Figure S1 (available in the supplemental material to this article), only four stations (BAD, CAE, DRE, and ZOU) were operating in 1996. The initial stations were originally equipped with short-period sensors. Over the years, broadband sensors gradually complemented or substituted the original instrumentation, whereas the equipment of the new stations always involved broadband sensors. In this study, we denote the recordings from both types of sensors with the same station name, except for station ZOU, which was changed to ZOU2 because of a slight contemporaneous change in location (few tens of meters and its installation in a borehole).
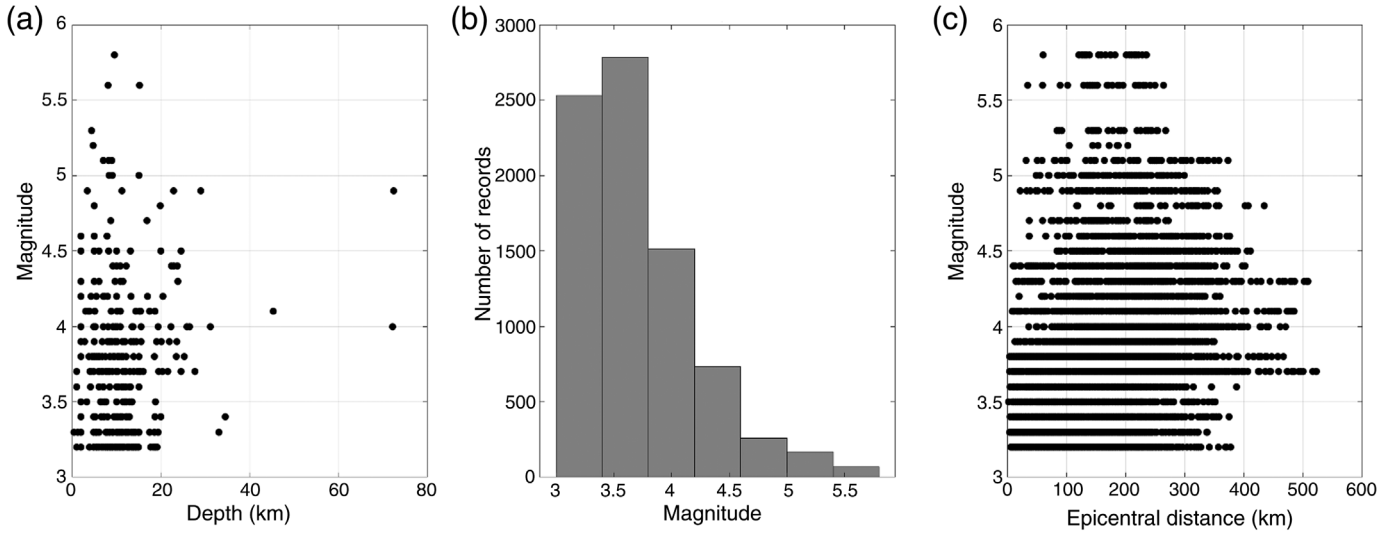
Figure 4 shows the number of earthquake recordings at some of the stations of the network along with the azimuth coverage. We observe an almost uniform azimuth coverage for stations that have been active for two decades and thus recorded a significant number of events (e.g., more than 300 at stations BAD, CAE, DRE, and ZOU). Stations that went into operation later recorded fewer events (less than 20 at stations ABSI, APGO, GAVI, GRDM, and QUIN), and their azimuth coverage is

irregular. The reader can find details regarding the instrumentation and site characteristics of the stations involved in this study in the OASIS (Priolo *et al.*, 2015).

Given the lack of shear-wave velocity data at most of the considered stations, we were unable to classify the sites with the usual mean shear-wave velocity from the surface to 30 m depth (V_{S30}) approach (Borcherdt, 1994), which is adopted as an international standard for soil classification in building code provisions. To evidence possible correlations between site response and site conditions, we considered two different site classification approaches. First, we considered the geomorphological scenarios proposed in Biolchi *et al.* (2011), which are defined according to the dominant topographical feature and the simple rock-soil dichotomy (Table 2). Second, we considered a set of soil classes corresponding to the prevalent local geology (Table 3).

Other data extracted from the recordings were the PGA and PGV, whereas we based seismic-noise-related studies on

4

Figure 3. Graphical representation of (a) magnitude versus depth, (b) the number of records versus magnitude, and (c) magnitude versus epicentral distance distributions that characterize the considered database.

180 min of spike-free seismic noise from the continuous recordings at each seismological station.

METHODS
NHV

As observed by Nakamura (1989), NHV could allow for the detection of the possible resonance frequency for shear waves. Because of its cost effectiveness, NHV has become a widespread tool for the analysis of site response in recent decades (Bard, 2008). However, several issues have prevented the scientific community from considering NHV as a strict quantitative proxy for the site-response function, as it was proposed in Nakamura (1989). Comparisons with other site-response estimation techniques (e.g., Pilz *et al.*, 2009) showed that NHV provides only a lower-frequency bound for site amplifications at the resonance frequency. On the other hand, specific NHV interpretation models, based on Rayleigh waves ellipticity (e.g., Fäh *et al.*, 2001), on the Airy phase of Love waves (e.g., Bonnefoy-Claudet *et al.*, 2008), or on body waves (Nakamura, 1989), explain data only in particular cases. Considering the diffuse field theory (Campillo and Paul, 2003) permits the interpretation of NHV in terms of the Green's tensor components for coinciding source and receiver (Sánchez-Sesma *et al.*, 2011), and some procedures that correct the horizontal-to-vertical ratio for direct amplification estimations have been proposed recently (Kawase *et al.*, 2019; Zhu *et al.*, 2020).

In the present study, we consider NHV data only as a supporting tool in the identification of the reference site candidates. We provide NHV data as part of station documentation without attempting any quantitative interpretation of the differences between NHV values and the site amplification function obtained with the GIT.

We evaluate the NHV ratio at each station in accordance with the guidelines provided in Picozzi *et al.* (2005) and the ones resulting from the Site EffectS assessment using AMbient Excitations (SESAME) project (Bard, 2008). For each station, we consider a population of about 50 200-second-long three-component stationary transients-free microtremor recordings. We calculate the NHV through the arithmetic mean of the logarithm of the ratio between the amplitude spectra of the horizontal and vertical components. We obtain the amplitude spectra of each recording as the square root of the power spectrum evaluated from the time series with the maximum entropy method.

Site amplification function based on GIT

We estimate the frequency-dependent site response by means of the GIT applied to the well-known source–path–site formal model, which expresses the shear-wave spectrum $U_{ij}(f)$ at a site i for an event j as

$$U_{ij}(f) = S_j(f)P(r_{ij}, f)H_i(f), \qquad (1)$$

in which $S_j(f)$ is the jth event source spectrum, $H_i(f)$ is the ith site-response function, $P(r, f)$ is the source-to-site path function, and r_{ij} is the source-to-site hypocentral distance. The model in equation (1) refers only to the far-field component of the ground motion. To exclude the spectral components corresponding to wavelengths larger than r_{ij}/π for the nearest events, we limited the spectral analysis of the data to the frequency range $f > 0.5$ Hz. Moreover, the model in equation (1) implies the linearity of the site response. If we exclude particular sites characterized by a layer of anthropogenic fill, which can exhibit a nonlinear response to weak motion (Di Giacomo *et al.*, 2005), the possibility of a nonlinear response is associated with motion with PGA exceeding 0.5 m/s^2 (Régnier *et al.*, 2013). Because the PGA of the recordings

TABLE 1
Housing, Outcropping Geology, Geomorphological Scenario, and Category of the Observed Seismic Response at Each of the 67 Stations

Station	Housing	Outcropping Geology	Geomorphological Scenario	Seismic Response Category
ABSI	Vault	PP-Pg	H-ss	B-band_Low
ACOM	Bunker	UP-Lb	H-cr	B-band_Low
ADRI	Vault	Q-Ap	S-fp	B-band_High
AFL	Vault	UT-Dp	H-cr	Deamplifying
AGOR	Mine	UP-Lb	H-ss	Neutral
APGO	Vault	Q-Am	S-sv	B-band_High
BAD	Vault	JC-Lm	H-ss	Neutral
BALD	Masonry hut	JC-Lm	H-cr	B-band_High
BOO	Vault	Q-Am	S-ms	B-band_Low
BOSI	Vault	Q-Am	S-dv	B-band_High
BUA	Vault	PE-Fl	S-fh	B-band_Low
CAE	Vault	JC-Lm	H-ss	Neutral
CARE	Vault	PP-Ps	H-ms	Neutral
CGRP	Bunker	JC-Lm	H-cr	B-band_Low
CIMO	Bunker	UT-Dp	H-ss	Deamplifying
CLUD	Mine	MT-Dl	H-es	Deamplifying
COLI	Vault	PE-Fl	H-ms	B-band_High
CSM	Vault	Q-Am	H-ss	Neutral
CSO	Vault	Q-Am	S-ss	B-band_Low
DOSS	Vault	JC-Lm	H-ms	B-band_High
DRE	Vault	PE-Fl	H-cr	B-band_High
ED01	Borehole (153 m)	Q-Ap	S-fp	B-band_Low
ED02	Borehole (33 m)	PQ-Cm	S-ms	Deamplifying
ED03	Borehole (32 m)	PQ-Cm	S-ms	B-band_Low
ED04	Borehole (27 m)	PQ-Cm	S-fh	B-band_Low
ED05	Borehole (10 m)	PQ-Cm	S-fh	B-band_Low
ED06	Borehole (5 m)	PQ-Cm	S-fh	B-band_High
ED07	Borehole (15 m)	PQ-Cm	S-fh	B-band_Low
ED08	Borehole (15 m)	PQ-Cm	S-fh	B-band_High
ED09	Borehole (15 m)	PQ-Cm	S-fh	B-band_Low
ED10	Borehole (14 m)	PQ-Cm	S-fh	N-band
FAU	Vault	PP-Ps	H-ss	Neutral
FERB	Borehole (130 m)	Q-Ap	S-fp	Neutral
FUSE	Vault	MT-Dl	H-es	Neutral
GAGG	Vault	Q-Am	S-ss	B-band_Low
GARG	Vault	JC-Lm	H-ss	Neutral
GAVI	Vault	Q-Am	S-sv	B-band_High
GAZZ	Vault	Q-Ap	S-fp	B-band_High
GRDM	Vault	JC-Lm	H-cr	B-band_High
IESO	Vault	Q-Ap	S-fp	B-band_High
KOSI	Vault	O-Bi	H-ss	B-band_Low
LSR	Vault	MT-Vo	H-cr	B-band_Low
LUSI	Vault	JC-Lm	H-cr	B-band_High
MARN	Vault	O-Bi	H-ss	B-band_High
MLN	Vault	JC-Lm	H-ss	Neutral
MOSI	Vault	PP-Ps	H-ss	B-band_Low
MPRI	Vault	JC-Lm	H-fp	Neutral
MTLO	Vault	PE-Fl	H-ms	N-band
OZOL	Vault	UT-Dp	H-ss	B-band_High
PANI	Bunker	PP-Ps	H-ms	B-band_Low
PLRO	Vault	UC-La	H-ss	B-band_High
PRED	Mine	UT-Dp	H-ss	Deamplifying
QUIN	Vault	Q-Ap	S-fp	B-band_High
RISI	Vault	PP-Ps	H-ms	B-band_High
RONC	Vault	JC-Lm	H-ms	N-band

TABLE 1 (Continued)				
Station	**Housing**	**Outcropping Geology**	**Geomorphological Scenario**	**Seismic Response Category**
ROSI	Vault	PP-Ps	H-ms	B-band_Low
SABO	Bunker	JC-Lm	H-ss	B-band_High
STIN (STI0)	Vault	Q-Ap	S-fp	B-band_High
STIN (STI1)	Borehole (100 m)	Q-Ap	S-fp	B-band_Low
TEOL	Masonry hut	PE-Fl	H-ms	N-band
TRI	Cave	JC-Lm	H-fp	B-band_Low
VARA	Vault	JC-Lm	H-ss	B-band_High
VARN	Vault	JC-Lm	H-ms	B-band_High
VINO	Cave	JC-Lm	H-ms	Neutral
ZIAN	Vault	O-Bi	H-ms	B-band_Low
ZOU	Vault	UC-La	H-cr	Deamplifying
ZOU2	Borehole (10 m)	UC-La	H-cr	Deamplifying

The acronyms for geomorphological scenarios and outcropping geology are given in Tables 2 and 3, respectively. The seismic response categories are described in the Results section.

considered in the present work does not exceed 0.2 m/s² (see Fig. 5), we can reasonably assume that the linear response model is valid for our analysis.

In solving equation (1), we do not postulate any model for the source or for the site terms, and due to the availability of a rich dataset that allows for a satisfactory coverage of the source-to-site distance range, we consider an inversion approach, which does not postulate any model for the path term. This approach, introduced by Castro et al. (1990), relies on the discretization of the distance domain in a number of nonoverlapping intervals. We express the model that we solve for in linear form as

$$\ln |U_{ij}^k(f)| = \ln |S_j(f)| + \ln |P_{l(i,j)}(f)| + \ln |H_i^k(f)|, \quad (2)$$

in which ln is the natural logarithm, k indicates one of the three spatial components of the ground motion, $l(i,j)$ indicates the distance interval corresponding to the i-j station–source pair,

and |-| denotes the absolute value. In the present study, we are interested in the components $|H_i^k(f)|$, which we call site amplification functions and result as the most robust part of the solution (e.g., Parolai et al., 2000). We allow for a dependence of the site terms in respect to the spatial component of the ground motion, whereas we assume only the source and propagation terms to be isotropic.

We solve the overdetermined linear system represented in equation (2) with the one-step generalized inversion approach (Oth et al., 2011), which we implemented in an improved version of the GITANES (GIT ANalysis of Earthquake Spectra) MATLAB package (Klin et al., 2018). To obtain a unique solution for the system in equation (2), we complement

| TABLE 2		
Acronyms for the 11 Geomorphological Scenarios Used to Classify the Station Sites—Simplified from Biolchi et al. (2011)		
Geomorphological Scenarios	**Rock (Vs > 800 m/s)**	**Soil (Vs < 800 m/s)**
Flat plain (slope < 8°)	H-fp	S-fp
Moderate slope (8° < slope < 15°)	H-ms	S-ms
Steep slope (slope > 15°)	H-ss	S-ss
Foothill (slope < 8°)		S-fh
Shallow valley (sides slope > 15°, width < 250 m, soil thickness < 30 m)		S-sv
Deep valley (sides slope > 15°, width > 250 m, soil thickness > 30 m)		S-dv
Edge of scarp	H-es	
Crest	H-cr	

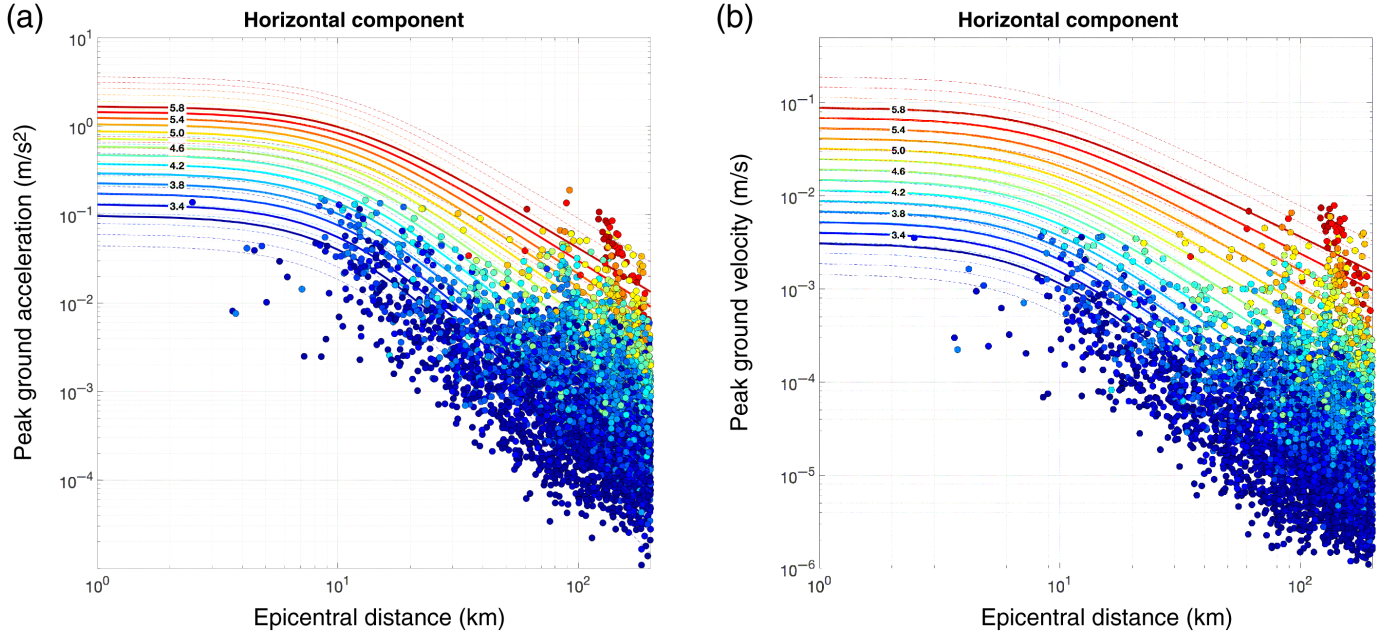| TABLE 3		
Acronyms for the Outcropping Geology at Station Sites		
Geological Description	**Age**	**Acronym**
Fluvioglacial and alluvial sediments of the alluvial plain	Quaternary	Q-Ap
Fluvioglacial and alluvial sediments of the mountains	Quaternary	Q-Am
Polygenic and heterometric conglomerates, marls, and siltstones	Plio-Quaternary	PQ-Cm
Volcanic rocks (basalts, ignimbrites)	Oligocene	O-Bi
Sandstone-shale alternations (Flysch)	Paleocene–Eocene	PE-Fl
Micritic limestones, basins deposits	Jurassic–Cretaceous	JC-Lm
Dolostones, shallow water carbonatic platform	Upper Triassic	UT-Dp
Basic volcanites	Medium Triassic	MT-Vo
Massive dolostones and dolomitic limestones	Lower-Medium Triassic	LT-Dl
Varicolored shales	Lower Triassic	LT-We
Bioclastic limestones	Upper Permian	UP-Lb
Hyaloclastites, diabases, and basaltic lavas	Upper Carboniferous	UC-La
Basement, paragneiss, and schists	Pre-Paleozoic	PP-Ps
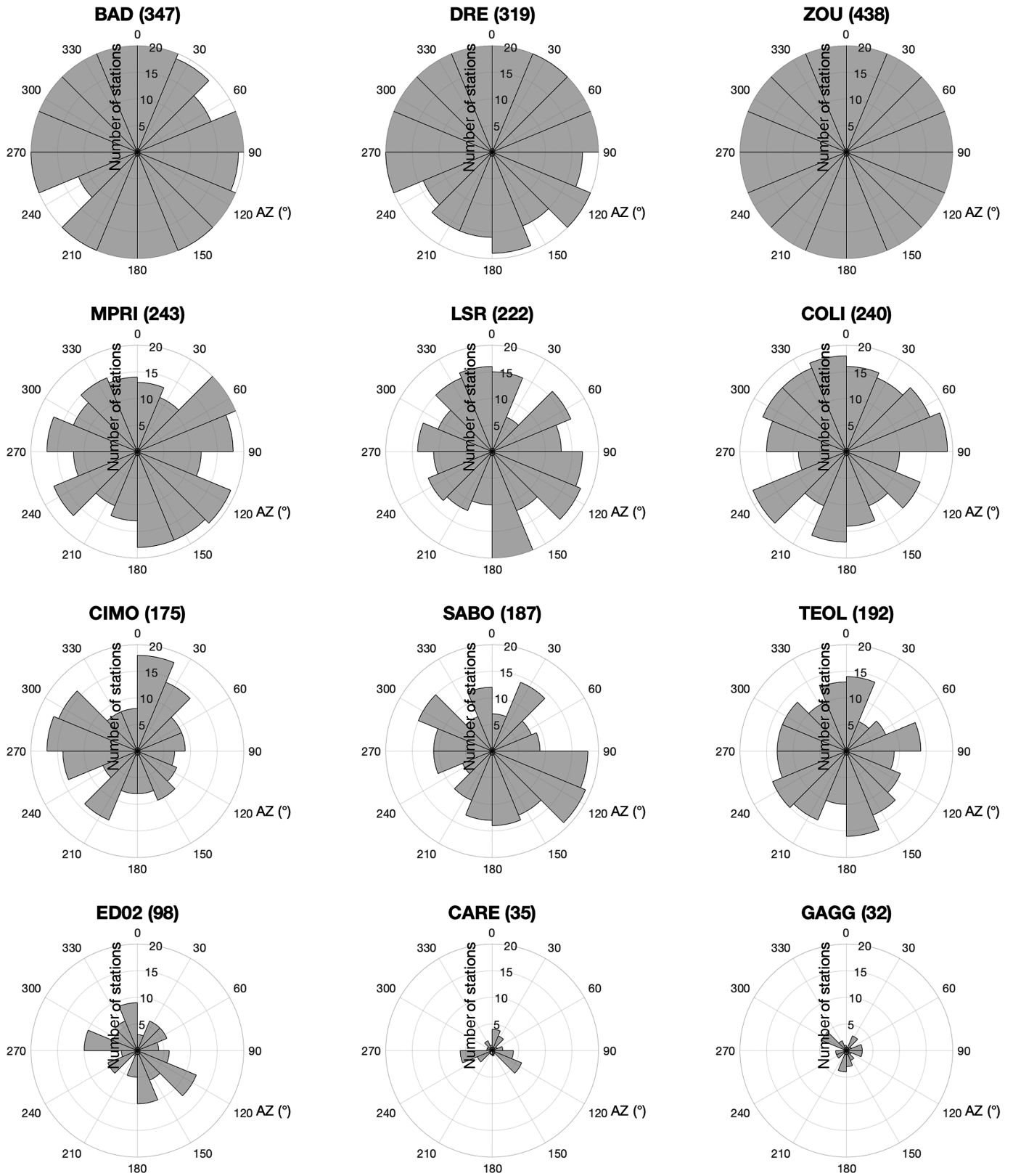
Figure 4. The azimuth coverage and the total number of recorded events (in parentheses) are not uniform across the stations, as can be seen in these polar plots considering a selection of stations. Only stations that have been active for several years (BAD, DRE, and ZOU in these examples have been active from 1996) present a large number of recordings with a nearly homogeneous azimuth coverage.

Figure 5. The horizontal ground-motion parameters extracted from the database as a function of epicentral distance and magnitude (colored dots) in comparison with the ground-motion prediction equation (GMPE) curves of Bindi *et al.* (2011). (a) Peak ground acceleration (PGA) and (b) peak ground velocity (PGV). The color version of this figure is available only in the electronic edition.

it with additional constraints. The usual choice is the imposition of a constraint relative to the site terms and the propagation terms. Typically, the site term constraint consists of the imposition of a reference station, which we assume to be free of site effects. For example, we impose the following condition:

$$\ln |H^{\mathrm{NS}}_{i_{\mathrm{ref}}}(f)| + \ln |H^{\mathrm{EW}}_{i_{\mathrm{ref}}}(f)| = 0, \tag{3}$$

which implies that the obtained amplification functions are relative to the geometrical mean of the two horizontal components in station i_{ref}.

Similarly, we impose the constraint relative to the propagation terms with the definition of a reference distance indicated by the index value l_{ref} by setting:

$$\ln |P_{l_{\mathrm{ref}}}(f)| = 0. \tag{4}$$

We also impose a smoothing variation in the path response between contiguous distance intervals by adding to the system the following constraint (Castro *et al.*, 1990):

$$2\ln |P_l(f)| - (\ln |P_{l-1}(f)| + \ln |P_{l+1}(f)|) = 0;$$
$$\text{with} \quad 1 < l < L, \tag{5}$$

in which L is the number of distance intervals.

To analyze the site response in terms of the FAS, we extract an adequate time window from the ground-motion recordings. In this study, we aim at the expected value of the site-specific spectral response for incoming S waves without distinction of the phase of the S wave and the causes of the change in the spectral content of the ground motion, as long as they are ascribable to specific physical conditions in the spatial neighborhood of the station. In addition to the site response to the

direct wave, we consider the response to later phases, that is, the sequence of reflections and refractions of the same shear impulse radiated from the seismic source. We also include in the response the possible basin-edge-induced surface waves (Semblat *et al.*, 2005), which might considerably increase the duration of ground motion (Pilz *et al.*, 2018). Buried heterogeneities in the basin structure may induce similar short-period surface waves also in parts of the alluvial plain that are far from the edges, as shown in Klin *et al.* (2019). Given the distance range of the analyzed events, we evaluate the FAS over a 64-second-long time window to include possible late phases in the response. We set the window starting point 2 s before the first S arrival and apply a 2-second-long cosine taper on both ends of the extracted window to avoid the box-car effects. The considered frequency range, $f > 0.5$ Hz, excludes long-period surface waves from the analysis. We evaluate the FAS through the fast Fourier transform and subsequently interpolate it on a predefined set of logarithmically spaced frequency samples.

Site amplification factor in respect to a GMPE

The concept of the site amplification factor, which we use here as a third parameter to describe the site response, relies on a given empirical GMPE. Following Laurenzano *et al.* (2019), we define the amplification factor $\alpha_i(Y)$ for the ground-motion parameter Y at the ith site as

$$\alpha_i(Y) = 10^{\frac{1}{N_i}\sum_{j=1}^{N_i}\log Y_{ij}-\log Y_{ij}^0}, \qquad (6)$$

in which Y_{ij} is the ground-motion parameter value estimated from the recording at the ith site for the jth event, Y_{ij}^0 is the corresponding median prediction of the GMPE, and N_i is the number of events recorded at the ith site. A lognormal distribution for the ratios Y_{ij}/Y_{ij}^0 at the ith site is postulated. In analogy to the terminology used by Spudich *et al.* (1999), we refer to the logarithm of the amplification factor as the station bias.

In the present work, we consider as ground-motion parameters Y the PGA and PGV. Given the geographical extension of the considered area and its variety in seismological, morphological, and tectonical styles, we chose to estimate the reference values Y_{ij}^0 with the GMPE ITA10 (Bindi *et al.*, 2011), which is based on strong-motion records from the entire Italian territory. In particular, we consider the ITA10 predictions for Eurocode 8 soil class A (Eurocode 8, 2004). Because ITA10 is derived considering distances up to 200 km, we limited the analysis of the site amplification factor to events with shorter distances. In Figure 5, we plot the values of the PGA and PGV extracted from the dataset (colored dots) against ITA10 as a function of the distances for different magnitude values. Even though ITA10 is calibrated for the magnitude range M 4.0–6.9, in this study we apply it also to events with slightly lower magnitude values (M >3.2) to allow for considering a statistically significant number of events at each station. The determination of reference ground-motion values for low-magnitude events by extending ITA10 below its lower calibration magnitude was already successfully applied in Laurenzano *et al.* (2019).

RESULTS

We analyzed the site response at the permanent stations in northeastern Italy through the following steps:

- selection of a reference station on the basis of the NHV;
- evaluation of the amplification functions for different components at each station with respect to the reference station by means of GIT; and
- evaluation of the amplification factors for PGV and PGA at each station and their comparison with the amplification functions.

The constraint concerning the reference station involves the assumption that site effects do not affect it. By applying this constraint, we understand the site-response solutions at non-reference stations as a relative site response with respect to the reference station. To permit a straight interpretation of the results, it is convenient to assign the reference site status to a station for which independent observations support the assumption of a neutral site response. In this study, we selected FAU as the reference station because it exhibits the flattest NHV ratio among all considered stations (see Fig. 6). We

estimate the flatness of the NHV ratio through its standard deviation over the frequency band 0.5–20 Hz. Because in our approach we consider the spatial components of the ground motion separately, we impose the reference site constraint on the combination of the two horizontal components (equation 3) at FAU.

To apply the GIT, we partition the distance range 7–300 km that characterizes the database into 29 intervals 10.1 km in width, with the population in each interval ranging from 65 to 427 three-component signals (Fig. S2). For the sake of simplicity, we select the first distance interval as the reference distance (i.e., we put $l_{\mathrm{ref}} = 1$ in equation 4).

In this study, we focus on the GIT solutions concerning the parameters $|H_i^{\mathrm{EW}}|$, $|H_i^{\mathrm{NS}}|$, and $|H_i^{\mathrm{UD}}|$ in equation (2).

We analyze the stations in terms of the amplification function $H(f)$ defined as the geometrical mean of the two horizontal components:

$$H(f) = (|H^{\mathrm{EW}}(f)|\,|H^{\mathrm{NS}}(f)|)^{\frac{1}{2}}. \qquad (7)$$

We consider the minimum and maximum value ($H_{\min}$ and $H_{\max}$, respectively) of $H(f)$ over the considered frequency band and the mean value $<H>$ defined as

$$\langle H \rangle = \exp\left(\frac{\int_{\ln(f_A)}^{\ln(f_B)} \ln(H(f))\,d\ln(f)}{\ln(f_B) - \ln(f_A)}\right), \qquad (8)$$

with $f_A = 0.5$ Hz and $f_B = 20$ Hz being the extremes of the considered frequency band. From Figure 7, it appears that only a relative majority (46%) of stations present moderate values of $<H>$ (i.e., $<H>$ above 1 but not exceeding 2) and 39% are affected by a relevant amplification ($<H>$ above 2).
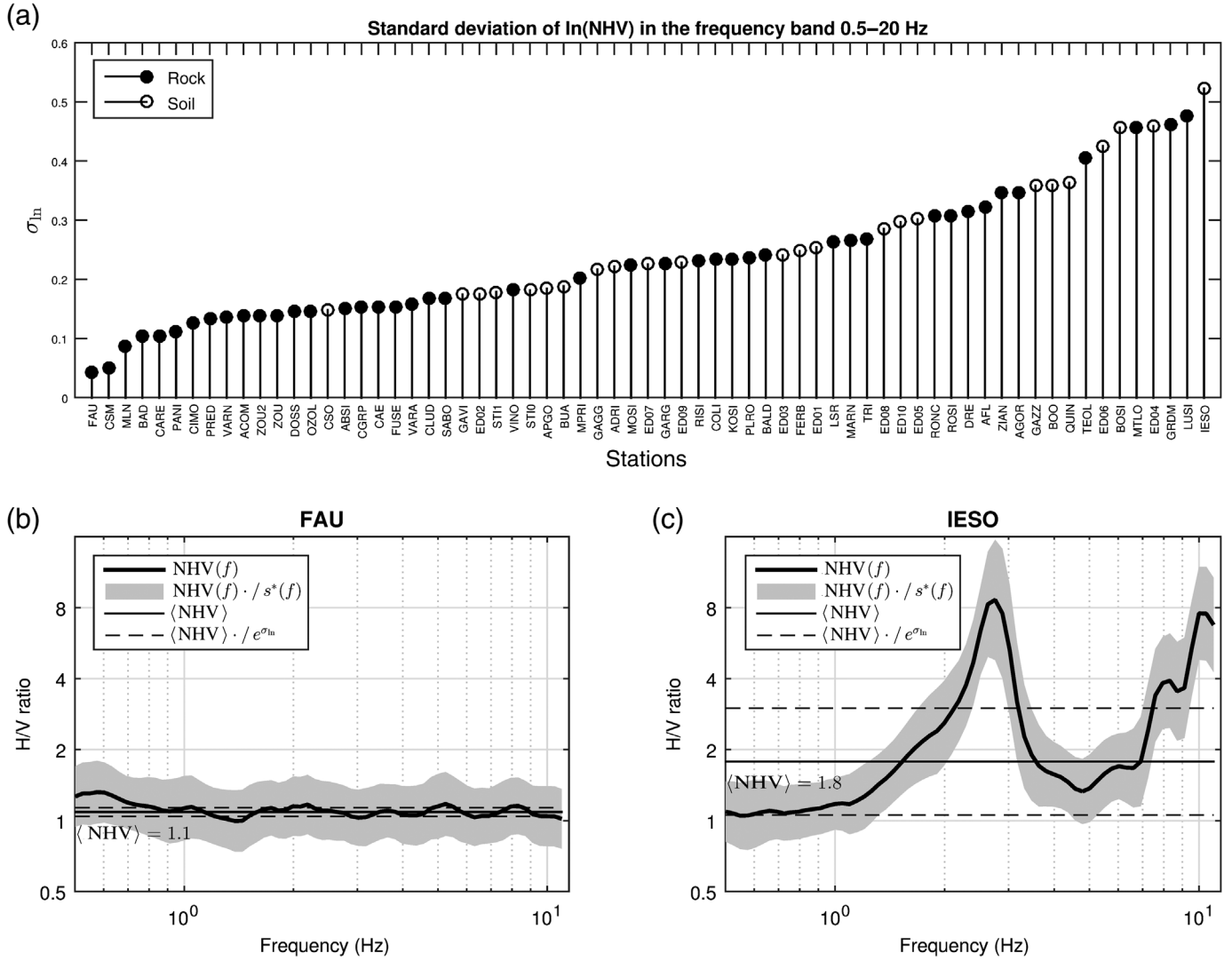
To recognize the amplification functions characterized by a prominent peak, we check for the following condition:

$$(H_{\max} H_{\min})^{\frac{1}{2}} > H. \qquad (9)$$

If equation (9) is verified, we describe the peak with the frequency f_{peak} corresponding to the peak value $H_{\max}$ and the two extremes f_1 and f_2 of the f_{peak} neighborhood in which $H(f) > <H>$. If both f_1 and f_2 are found in the (f_A, f_B) interval, we measure the width of the peak with the ratio f_2/f_1; otherwise, a "broadband" character of the peak is assigned.

On the basis of the values of the parameters $H_{\min}$, $H_{\max}$, $<H>$, f_1, and f_2, we were able to group the various amplification function behaviors into the following five categories:

- neutral amplification, with $H_{\min} \geq 0.5$ and $H_{\max} \leq 2$ (12 stations, including FAU);
- narrowband amplification, with equation (9) satisfied, f_1 and f_2 within 0.5–20 Hz and $H_{\max} > 2$ (four stations);
- deamplification, with $<H> < 1$ (seven stations);

Figure 6. (a) The flatness of the noise horizontal-to-vertical (H/V) spectral ratio (NHV) at each station is evaluated in terms of standard deviation σ_{ln} of the NHV's logarithm over the considered frequency band. (b) At station FAU, the NHV displays the lowest deviations from its median <NHV> over the frequency band. (c) At station IESO, the NHV presents the highest deviations. The symbol "·/" stands for "times or divided by," whereas "$s*$" is the multiplicative standard deviation of the NHV's measure.

- broadband low amplification, with $1 \leq \langle H \rangle \leq 2$ (21 stations); and
- broadband high amplification, with $\langle H \rangle > 2$ (23 stations).

To recognize possible correlations between the quantitative site response and the site conditions, we show in Figure 8 the distribution of the five site-response categories versus the two site classifications defined in the Stations and Data section. Although no plot suggests strict equivalence between amplification categories and site typologies, we can note some trends. The neutral amplification appears related to the rock steep slope geomorphological scenario and Jurassic–Cretaceus limestones, whereas deamplification occurs at sites characterized by dolostones and limestones of older age. Narrowband amplification unexpectedly occurs mainly at rock sites. On the other hand, the numerous sites characterized by broadband (either high or low) amplification are distributed among different geomorphological and geological types without a clear pattern. We can also note how stations located on a crest display different behaviors, ranging from broadband high amplification to

deamplification, suggesting the presence of not easily predictable topographic effects (Burjánek et al., 2014).

To gain additional information on the site-response behavior, we consider the GIT solution concerning the vertical component $|H^{\text{UD}}(f)|$, which measures the vertical amplification at each station in respect to the horizontal motion at the reference station. This parameter allows us to evaluate the EHV (Lermo and Chávez-García, 1993). In fact, if we express the logarithm of EHV as

$$\ln \text{EHV} = \frac{1}{N} \sum_{j=1}^{N} \ln \left(\frac{(|U_j^{\text{EW}}| \, |U_j^{\text{NS}}|)^{\frac{1}{2}}}{|U_j^{\text{UD}}|} \right), \qquad (10)$$
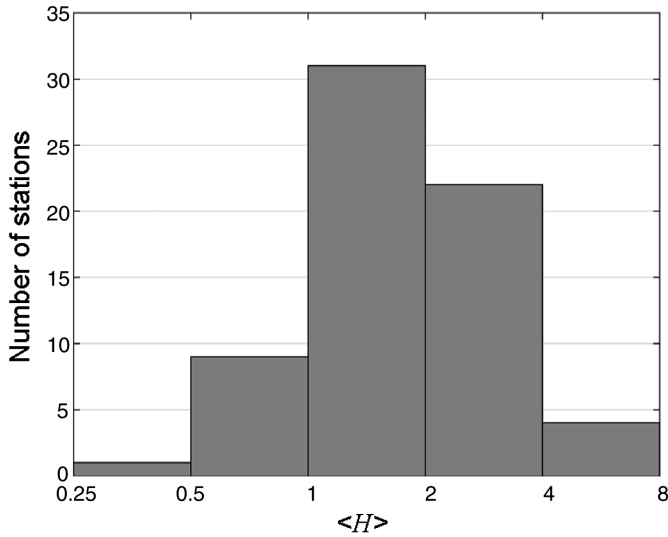
Figure 7. The 67 permanent stations in northeastern Italy present a broad range of values for the mean horizontal amplification $<H>$ over the frequency band 0.5–20 Hz. In total, 31 stations (46%) are characterized by an overall moderate amplification ($1< <H> < 2$), 10 stations (15%) present deamplification ($<H> < 1$), and 26 stations (39%) present high amplification levels ($<H> > 2$).

Figure 8. The occurrence of different site-response typologies (see the Results section) in respect to (a) geomorphological scenarios as defined in Table 2 and (b) surface geology as defined in Table 3. The color version of this figure is available only in the electronic edition.

with N being the number of events recorded at the station and $|U_j^{EW}|$, $|U_j^{NS}|$, and $|U_j^{UD}|$ being the amplitude spectra of the ground-motion components for the jth event and if we substitute equations (2) and (7) in equation (10), we obtain

$$\text{EHV}(f) = \frac{H(f)}{H^{UD}(f)}. \tag{11}$$

In Figures 9–13, we show three examples for each of the five amplification function categories. For comparison, we also add the EHV ratio evaluated from the GIT solution through equation (11) (in blue) and the NHV ratio (in red).

In Figure 9, we see three examples of sites that behave similarly to the chosen reference station FAU and that can possibly play this role equally well. We can observe in Figure 9a that, even though AGOR presents a peak, its amplitude is below 2; therefore, it does not fully satisfy our criteria describing the narrowband amplification. AGOR would be classified in the narrowband category if we considered either EHV or NHV —both exhibit larger peak values than $H(f)$—as the amplification function instead of $H(f)$. In Figure 9b, concerning the borehole station FERB (located under 100 m of sediments in the Po Plain) the EHV, NHV, and $H(f)$ curves do not match well and present a series of peaks and notches, which are emphasized by the logarithmic scale of the plot but are confined in the 0.5–2 value interval. We can attribute the regular succession of peaks and notches in $H(f)$ to the contamination from the reflected phase at the free surface (Bonilla et al., 2002). In Figure 9c, describing station VINO, which is located on rock in a natural cave, the EHV, NHV, and $H(f)$ curves appear more stable and almost match each other.

In Figures 10a–c, we plot three examples of "narrowband" amplification, that is, the stations MTLO, RONC, and TEOL, respectively, which are all installed on rock sites. In all three cases, the EHV and NHV curves identify the same peak of the $H(f)$ curve, but their values are considerably lower. The causes of the amplification peak at these stations are not yet clear to us.

In Figures 11a–c, we present three out of seven cases of "deamplifying" stations, one for a station on the surface (AFL), one in a mine (PRED), and
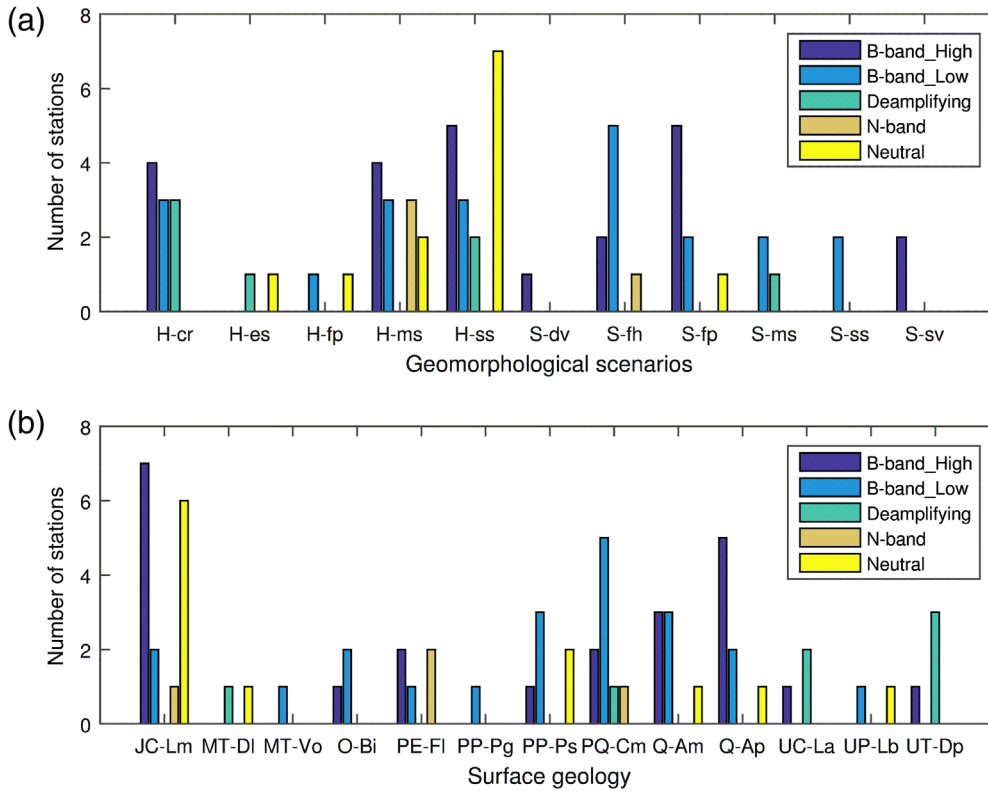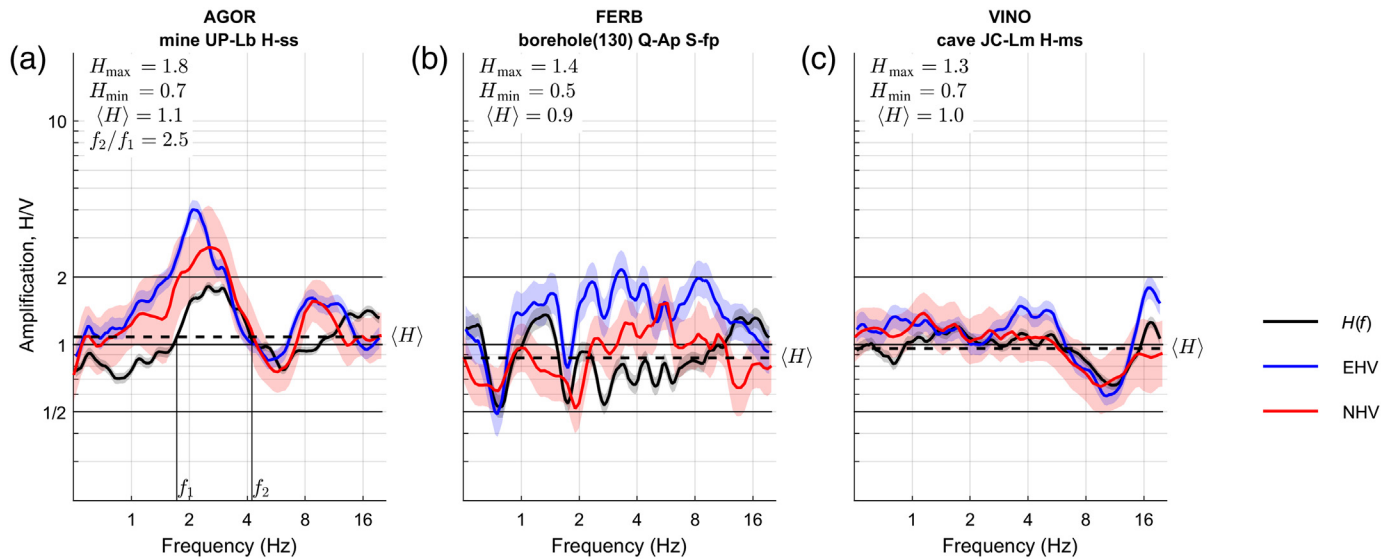
Figure 9. Three examples of "neutral" station category (see the Results section for categories description). (a) AGOR in the experimental mine in the Agordo municipality in the Dolomites, (b) FERB in a 130 m deep borehole in the Po Plain near the city of Ferrara, and (c) VINO in the Villanova natural cave in the Julian Alps. Each panel shows the horizontal amplification function $H(f)$ and the H/V ratio calculated from earthquakes (EHV) and NHV. The logarithmic scale emphasizes the differences between the curves in the value range around unity. The shadowed areas represent the standard error. The color version of this figure is available only in the electronic edition.
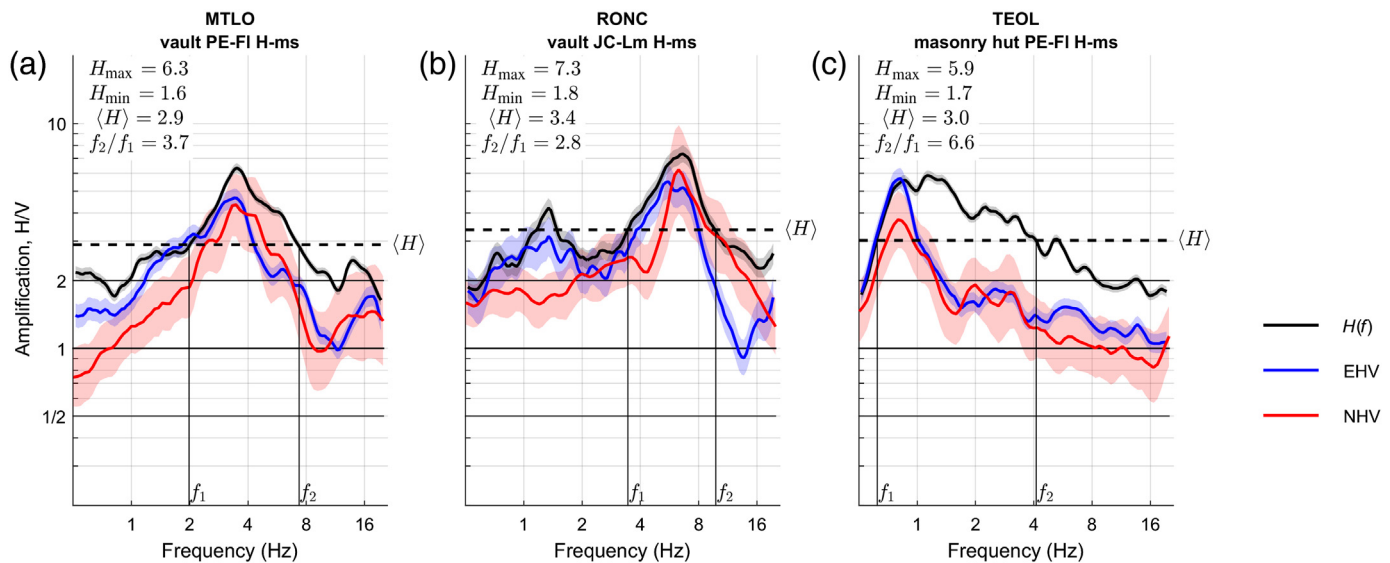
Figure 10. Three examples of "narrowband amplification" station (see the Results section for station categories description). (a) MTLO on the Montello hill in the Venetian Plain, (b) RONC on a slope near the Roncone municipality in the Southern Rhaetian Alps, and (c) TEOL near the Teolo municipality in the Euganean Hills. Other details as in Figure 9. The color version of this figure is available only in the electronic edition.

one in a shallow borehole (ZOU2). In all three cases, the deamplification occurs as a progressive lowering of the $H(f)$ curve with the frequency, whereas EHV and NHV match each other and remain at higher values. The deamplification for the surface and shallow borehole stations could be due to their installation on a medium that is stiffer than the one at the reference station and thus presents a relatively lower rock site amplification (Boore and Joyner, 1997). Such relative deamplification occurs on the vertical component as well, implying the discrepancy between the $H(f)$ curve on one side and NHV and EHV on the other.

In Figures 12a–c, we present three examples of stations with low broadband amplification. To this group belongs also the deep borehole station STI1. Contrary to the similar FERB case, the reflected phases at the free surface generate peaks that are high enough to classify STI1 as an amplifying station. It follows that the deployment of seismic sensors at depth does not ensure

13
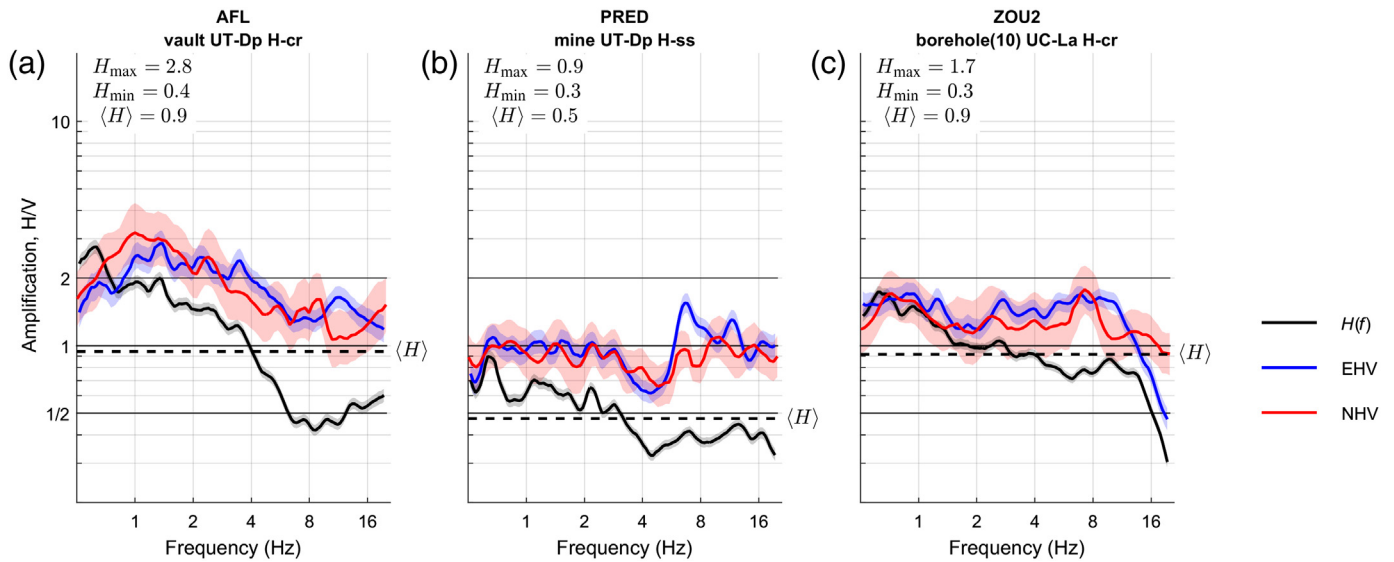
Figure 11. Three examples of station with "deamplification" (see the Results section for station categories description). (a) AFL on the crest of the Alpe Faloria mountain in the Dolomites, (b) PRED in the Predil former mine in the Julian Alps, and (c) ZOU in a 10 m deep borehole near the top of the Zoufplan mountain in the Carnic Alps. Other details as in Figure 9. The color version of this figure is available only in the electronic edition.
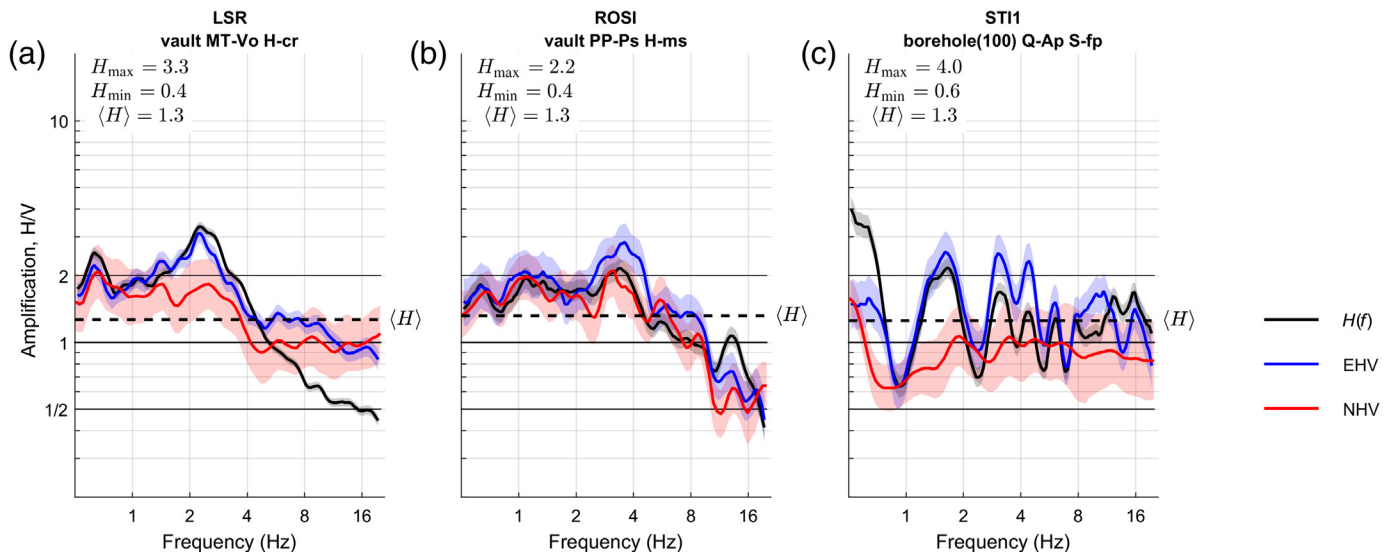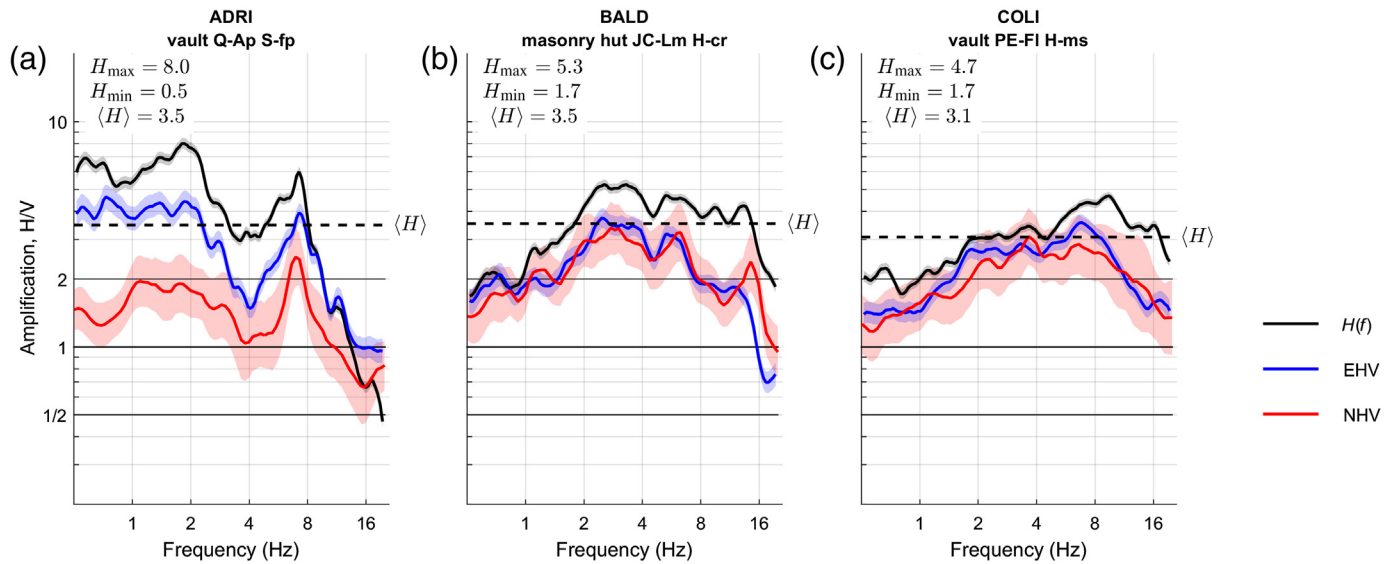

Figure 12. Three examples of "broadband low amplification" station (see the Results section for station categories description). (a) LSR on the Lussari mountain in the Julian Alps, (b) ROSI on the Rosskopf mountain in the Stubai Alps, and (c) STIN with sensor in a 100 m deep borehole near San Stino di Livenza municipality in the Venetian plain. Other details as in Figure 9. The color version of this figure is available only in the electronic edition.

recordings free of site effects and that the interpretation of the signals recorded in boreholes must be undertaken with appropriate methods (Parolai *et al.*, 2009; Laurenzano *et al.*, 2017).

The last three examples in Figure 13 concern high broadband amplification. Whereas this category of amplification is plausible for surface stations such as ADRI, which is located in the Po Plain basin, it is unexpected for a rock site such as BALD and COLI. In considering that $H(f)$ at BALD exhibits a plateau between 2 and 16 Hz, we can explain this behavior with topographic effects (BALD is on a mountain crest), with the housing (BALD is installed in a masonry hut), or with a combination of both effects. On the other hand, the amplification at COLI is probably due to the relatively young age of surface geology. In all three cases, $H(f)$ exhibits higher values than EHV and NHV. EHV and NHV practically match at BALD and COLI, whereas at ADRI they are characterized by a gap between EHV and NHV ratios, which slowly decreases with frequency.

Figure 13. Three examples of "broadband high amplification" station (see the Results section for station categories description). (a) ADRI near the town Adria in the Po Plain, (b) BALD on the Monte Baldo mountain range, and (c) COLI in the Colloredo di Monte Albano municipality in Friuli. Other details as in Figure 9. The color version of this figure is available only in the electronic edition.
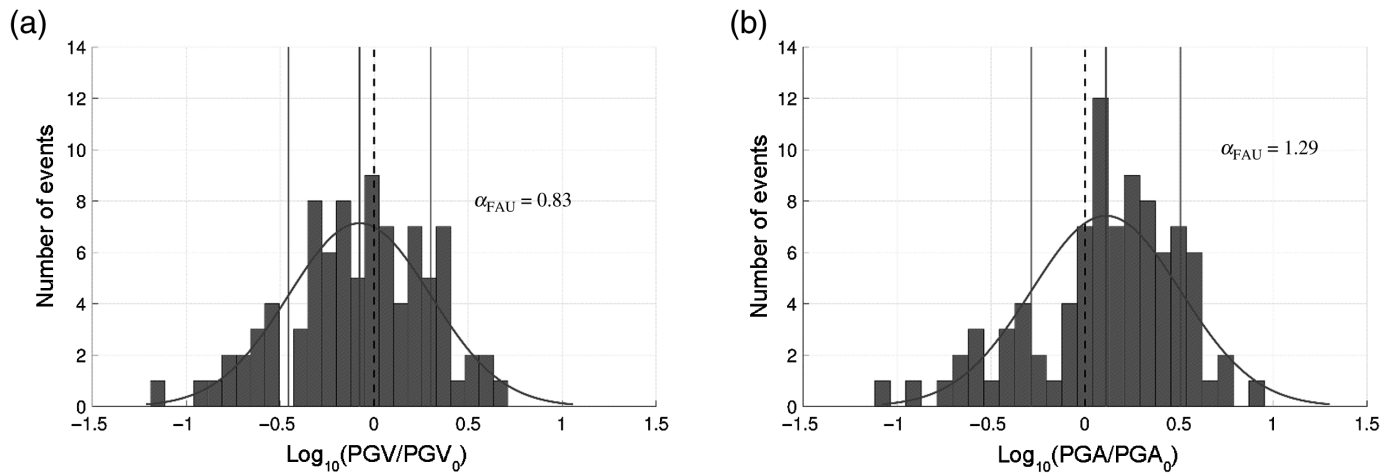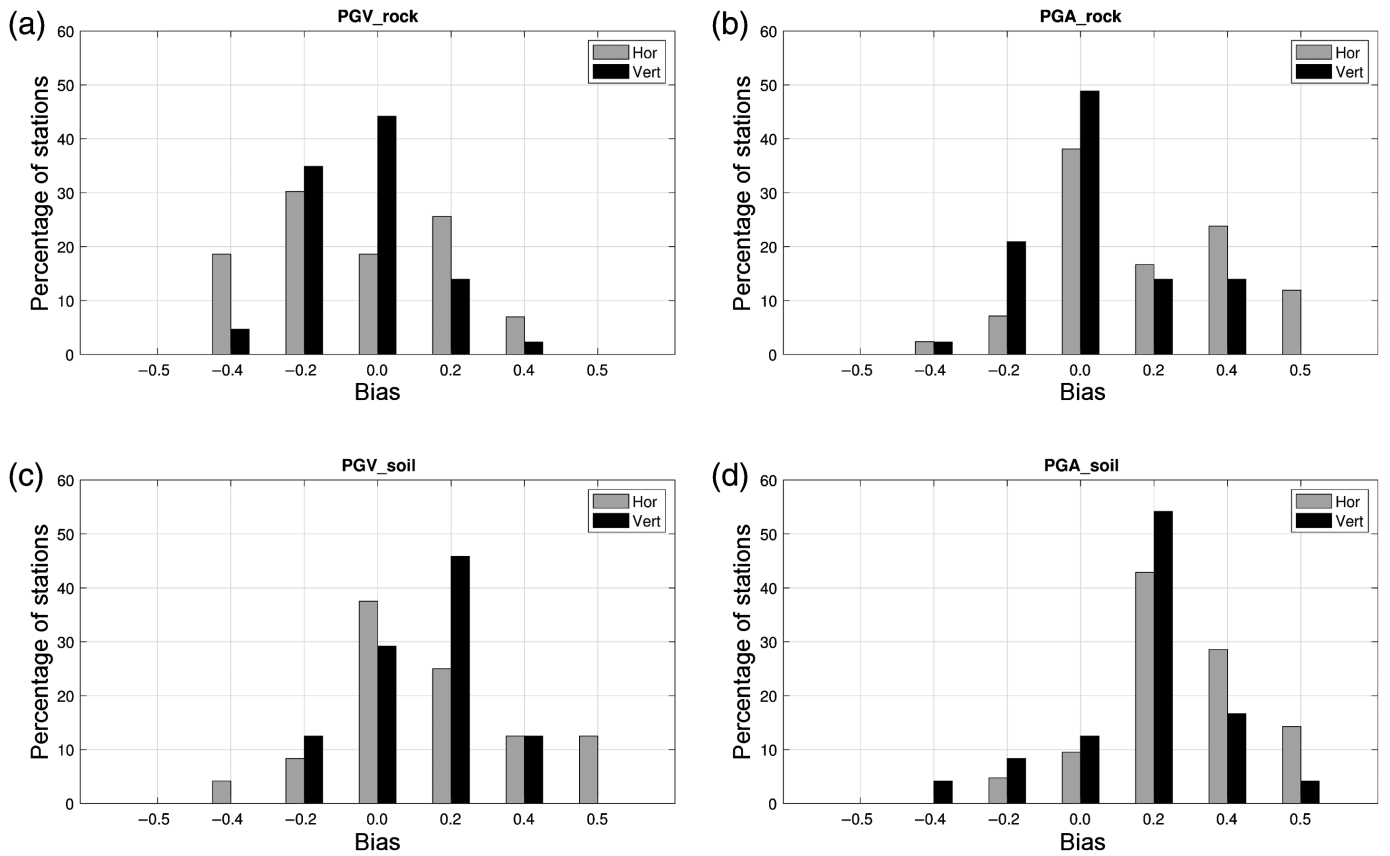

Figure 14. Distribution of the logarithm of the ratio between the observed and the GMPE-predicted peak ground-motion values at station FAU: (a) PGV and (b) PGA. The amplification factor α_{FAU} is the geometrical mean of the ratio and is near unity in both cases.

The amplification functions obtained at all 67 stations are plotted in Figures S4–S13. The results regarding the site response at five stations that were operative in 1996 (i.e., BAD, CAE, DRE, and ZOU) are in good agreement with the results presented in Malagnini *et al.* (2004).

In addition to the estimation of the frequency-dependent amplification functions with respect to the reference station FAU, we evaluated the amplification factors α, as defined in equation (6), for PGA and PGV with respect to the GMPE ITA10 for Eurocode 8 site class A (Bindi *et al.*, 2011). As an example, we represent in Figure 14 the distribution of the ratio between the measured and predicted ground-motion parameters at station FAU. We can observe that both the PGA and PGV amplification factor distributions feature a lognormal shape with median near 1 ($\alpha(PGV) = 0.83$ and $\alpha(PGA) = 1.29$). However, Figure 15 evidences that only a limited fraction of stations presents an amplification factor near unity. The central bin of the histograms, which samples the values of α ranging approximately from 0.8 to 1.25, represents a little less than 20% and 40% of the total number of stations on rock sites for the horizontal PGV and PGA, respectively (and about 45% and 49% for the vertical PGV and PGA, respectively). Most stations exhibit either positive or negative bias, a fact that is consistent with the variety of
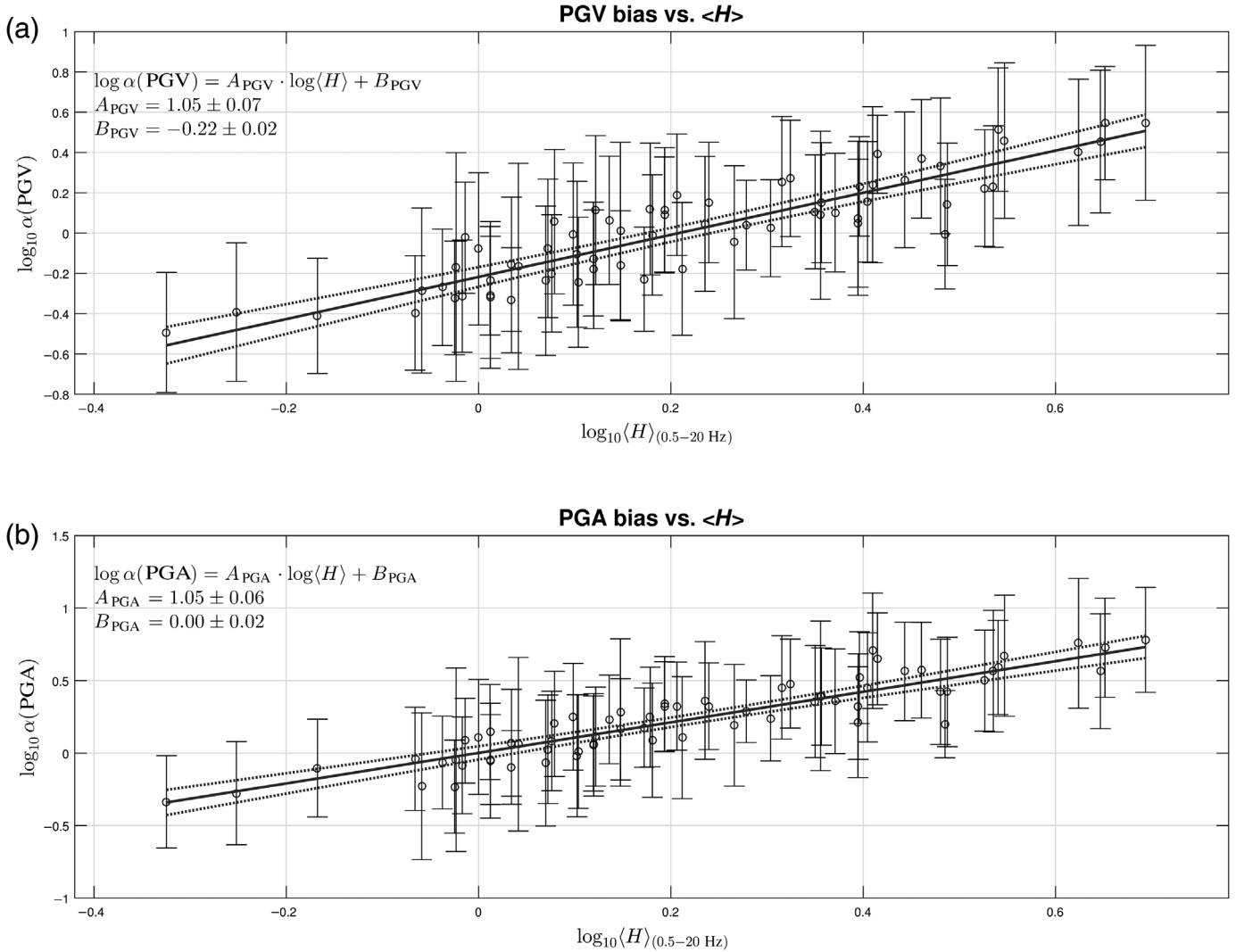
Figure 15. Histograms of station bias (base 10 logarithm of the amplification factor with respect to GMPE ITA10). (a) PGV at rock sites, (b) PGA at rock sites, (c) PGV at soil sites, and (d) PGA at soil sites. Horizontal and vertical amplification are compared on the same plot. The bins are labeled with the central value of the intervals. The bin width is 0.2.

amplification functions resulting from GIT. From Figure 15, it appears that stations on rock likely present a negative PGV bias, whereas PGA bias results are well balanced between positive and negative values. As expected, stations on soil (lower two plots in Fig. 15) present a dominance of positive values for both the PGA and PGV biases.

Figure S3 provides a station-by-station insight into the logarithm of the amplification factors and a picture of the variety in the site response that is similar to the one observed for the amplification function. To highlight the possible correlation between the two descriptions of the site effects, in Figure 16 we attempt a linear fit of the logarithm of amplification factors α(PGA) and α(PGV), respectively, against the logarithm of <H> for the horizontal component. The apparent proportionality between the amplification factors and the frequency-averaged amplification function suggests the possibility of employing the amplification functions that were obtained with GIT from weak-motion data in the estimation of amplification factors for ground-motion scenarios.

CONCLUSIONS

We estimated the seismic site response of 67 permanent stations located in northeast Italy, using 7361 three-component digital earthquake recordings that had been collected over a period of 20 yr. We expressed the site response in terms of Fourier spectral amplification functions with respect to the station FAU, which we selected as the reference station in virtue

of the flatness of the NHV. In addition, we computed the effect of the site response on the PGA and PGV, estimating their respective amplification factors with respect to the GMPE ITA10 (Bindi et al., 2011).

The determination of the amplification function relied on the conventional decomposition of the S-wave phase in terms of source, propagation, and site response. These terms were evaluated by a nonparametric approach through a single-step GIT in the frequency band 0.5–20 Hz.

We grouped the retrieved amplification functions into five categories. For each category, we provided three examples with a comparison between the amplification function with the EHV and NHV. We found that only 11 out of 66 stations belong to the "neutral" category (i.e., amplification function with values bounded in the interval 0.5–2 and that can be assumed flat and unitary with respect to station FAU). A minor percentage (7%) exhibit a narrowband amplification, whereas the majority of stations (44) belong to the categories of broadband amplification. In particular, 23 of these (34% of network stations) exhibit a mean amplification value larger than 2. This

(a) PGV bias vs. <H>

$$\log\alpha(\mathbf{PGV}) = A_{\mathrm{PGV}} \cdot \log\langle H \rangle + B_{\mathrm{PGV}}$$
$$A_{\mathrm{PGV}} = 1.05 \pm 0.07$$
$$B_{\mathrm{PGV}} = -0.22 \pm 0.02$$

y-axis: $\log_{10}\alpha(\mathrm{PGV})$
x-axis: $\log_{10}\langle H \rangle_{(0.5-20\ \mathrm{Hz})}$

(b) PGA bias vs. <H>

$$\log\alpha(\mathbf{PGA}) = A_{\mathrm{PGA}} \cdot \log\langle H \rangle + B_{\mathrm{PGA}}$$
$$A_{\mathrm{PGA}} = 1.05 \pm 0.06$$
$$B_{\mathrm{PGA}} = 0.00 \pm 0.02$$

y-axis: $\log_{10}\alpha(\mathrm{PGA})$
x-axis: $\log_{10}\langle H \rangle_{(0.5-20\ \mathrm{Hz})}$

Figure 16. Comparison of the mean value of the horizontal amplification function against the values of the amplification factor for (a) PGV and (b) PGA at each station and the correspondent linear fit on the logarithmic scale. Linear fit parameters are reported along with their standard errors, whereas the dotted curves delimit the 95% confidence interval of the fit.

finding is in accordance with a recent analysis that identified—on the basis of horizontal-to-vertical spectral ratios—exactly the same percentage of stations with large amplification in the Italian seismic network, run by Istituto Nazionale di Geofisica e Vulcanologia (Pischiutta *et al.*, 2018).

We discussed three examples of the amplification function for each of the five defined categories and compared them with NHV and EHV. However, the lack of seismic-velocity profiles prevented us from providing explanations in quantitative terms. The visual comparisons between the amplification function retrieved with GIT and the horizontal-to-vertical spectral ratios (either EHV or NHV) confirm that the latter are not always a reliable alternative to the reference site approach because they can either overestimate or underestimate the amplification function, in part or over the entire considered frequency band.

The analysis in terms of PGA and PGV amplification factors with respect to the GMPE ITA10 reveals that stations on rock likely present a negative PGV bias, whereas PGA bias results are equipartitioned between positive and negative values. Stations on soil present a dominance of positive values for both the PGA and PGV biases.

If we look at the occurrence of site-response categories in relation to 13 site geology classes and 11 site geomorphological scenarios, we observe that broadband amplification is distributed among different geomorphological and geological types without a clear pattern. On the other hand, stations characterized by the same geomorphological scenario display different behaviors; for example, stations on a crest could exhibit either broadband high amplification or deamplification. This observation is in accordance with the suggestion that seismic response at sites with pronounced topography could be more dependent on the subsurface seismic-velocity structure than on surface geometry (Burjánek *et al.*, 2014). The fact that site-response categories appear to fit with geological or geomorphological classes only in a limited number of cases questions the feasibility of rapid

site-response identification approaches based on terrain classification and evidences the need for subsurface investigation to explain the observed amplification functions.

Finally, we attempted a station-by-station comparison between the amplification function averaged over the 0.5–20 Hz frequency band and the PGA and PGV amplification factors and found encouraging results concerning the possibility of employing correction factors deduced from amplification functions in the calculation of the first-order ground-motion scenarios. Further study will be dedicated to better investigate this aspect.

The northeastern Italy network is not an exception among regional seismic networks worldwide in presenting a variety of site responses at its stations. The lack of seismic-velocity profiles often prevents the prediction of the site behavior, whereas the site classification using geology and/or geomorphologic features is not always reliable. The retrieval of the amplification functions with the application of GIT on a database of past recordings, as illustrated in the present work, therefore provides an advisable solution for the accurate interpretation of data from any regional network, in monitoring applications as well as in studies related to seismic hazard.

DATA AND RESOURCES

The seismic waveforms and station information were obtainable from the National Institute of Oceanography and Applied Geophysics (OGS) Archive System of Instrumental Seismology (OASIS) at http://oasis.crs.inogs.it (last access September 2020). The processed data belong to the following networks: the North-East Italy Seismic Network (OX, doi: 10.7914/SN/OX), the North-East Italy Broadband Network (NI, doi: 10.7914/SN/NI), the Trentino Seismic Network (ST, doi: 10.7914/SN/ST), the Collalto Seismic Network (EV, doi: 10.7914/SN/EV), and the Province Südtirol Network (SI). The mutual use of data recorded by different networks for scientific purposes is regulated by an agreement among different Institutions (OGS, Friuli-Venezia Giulia and Veneto Region, Provincia Autonoma di Trento, Land Tirol, and Alto Adige Civil Protection) within the project "Scambio dati sismici" (seismic data exchange). The supplemental material consists of 13 additional figures and three spreadsheets. The figures describe the timeline of events recorded at each station (Fig. S1), the distribution of recordings as a function of hypocentral distance (Fig. S2), station-by-station values of the amplification factors (Fig. S3), and the comparison among the amplification function $H(f)$, horizontal-to-vertical spectral ratio of earthquake recordings (EHV), and horizontal-to-vertical spectral ratio of noise recordings (NHV) for each of the 67 stations discussed in the article (Figs. S4–S13). The spreadsheets contain the tabulated amplification functions and factors for each station.

DECLARATION OF COMPETING INTERESTS

The authors declare no competing interests.

ACKNOWLEDGMENTS

REFERENCES

Ambraseys, N. N., K. A. Simpson, and J. J. Bommer (1996). Prediction of horizontal response spectra in Europe, *Earthq. Eng. Struct. Dynam.* **25,** no. 4, 371–400, doi: 10.1002/(SICI)1096-9845 (199604)25:4<371::AID-EQE550>3.0.CO;2-A.

Bard, P.-Y. (2008). The H/V technique: Capabilities and limitations based on the results of the SESAME project—Foreword, *Bull. Earthq. Eng.* **6,** no. 1, 1–2, doi: 10.1007/s10518-008-9059-4.

Bindi, D., F. Pacor, L. Luzi, R. Puglia, M. Massa, G. Ameri, and R. Paolucci (2011). Ground motion prediction equations derived from the Italian strong motion database, *Bull. Earthq. Eng.* **9,** no. 6, 1899–1920, doi: 10.1007/s10518-011-9313-z.

Biolchi, S., L. Zini, P. Leita, and P. Malisan (2011). Mapping the geomorphological scenarios of the Friuli Venezia Giulia region (NE Italy): A tool for the evaluation of the local seismic amplification, *Il Quaternario* **24,** 79–80.

Bonilla, L. F., J. H. Steidl, J.-C. Gariel, and R. J. Archuleta (2002). Borehole response studies at the Garner Valley Downhole Array, Southern California, *Bull. Seismol. Soc. Am.* **92,** no. 8, 3165–3179, doi: 10.1785/0120010235.

Bonnefoy-Claudet, S., A. Köhler, C. Cornou, M. Wathelet, and P.-Y. Bard (2008). Effects of Love waves on microtremor H/V ratio, *Bull. Seismol. Soc. Am.* **98,** no. 1, 288–300, doi: 10.1785/0120070063.

Boore, D. M. (2004). Can site response be predicted? *J. Earthq. Eng.* **8,** no. sup001, 1–41, doi: 10.1080/13632460409350520.

Boore, D. M., and W. B. Joyner (1997). Site amplifications for generic rock sites, *Bull. Seismol. Soc. Am.* **87,** no. 2, 327–341.

Borcherdt, R. D. (1994). Estimates of site-dependent response spectra for design (methodology and justification), *Earthq. Spectra* **10,** no. 4, 617–653, doi: 10.1193/1.1585791.

Bragato, P. L., and D. Slejko (2005). Empirical ground-motion attenuation relations for the Eastern Alps in the magnitude range 2.5–6.3, *Bull. Seismol. Soc. Am.* **95,** no. 1, 252–276, doi: 10.1785/0120030231.

Bragato, P. L., P. Comelli, A. Saraò, D. Zuliani, L. Moratto, V. Poggi, G. Rossi, C. Scaini, M. Sugan, C. Barnaba, *et al.* (2021). The OGS–Northeastern Italy Seismic and Deformation Network: Current Status and Outlook, *Seismol. Res. Lett.* **92,** doi: 10.1785/0220200372.

Burjánek, J., B. Edwards, and D. Fäh (2014). Empirical evidence of local seismic effects at sites with pronounced topography: A systematic approach, *Geophys. J. Int.* **197,** no. 1, 608–619, doi: 10.1093/gji/ggu014.

Campillo, M., and A. Paul (2003). Long-range correlations in the diffuse seismic coda, *Science* **299,** no. 5606, 547–549, doi: 10.1126/science.1078551.

Castellarin, A., R. Nicolich, R. Fantoni, L. Cantelli, M. Sella, and L. Selli (2006). Structure of the lithosphere beneath the Eastern Alps (southern sector of the TRANSALP transect), *Tectonophysics* **414,** no. 1, 259–282, doi: 10.1016/j.tecto.2005.10.013.

Castro, R. R., J. G. Anderson, and S. K. Singh (1990). Site response, attenuation and source spectra of S waves along the Guerrero, Mexico, subduction zone, *Bull. Seismol. Soc. Am.* **80,** no. 6A, 1481–1503.

Chen, Y., and Y. Wang (2018). Possible site effects revealed by regional earthquake records in the Qaidam Basin, China, *Seismol. Res. Lett.* **90,** no. 1, 280–293, doi: 10.1785/0220180095.

Di Giacomo, D., M. R. Gallipoli, M. Mucciarelli, S. Parolai, and S. M. Richwalski (2005). Analysis and modeling of HVSR in the presence of a velocity inversion: The case of Venosa, Italy, *Bull. Seismol. Soc. Am.* **95,** no. 6, 2364–2372, doi: 10.1785/0120040242.

Drouet, S., F. Cotton, and P. Guéguen (2010). v_{S30}, κ, regional attenuation and M_w from accelerograms: Application to magnitude 3–5 French earthquakes, *Geophys. J. Int.* **182,** no. 2, 880–898, doi: 10.1111/j.1365-246X.2010.04626.x.

Eurocode 8 (2004). Eurocode 8: Design of structures for earthquake resistance, Part 1: General rules, seismic actions and rules for buildings, EN 1998-1:2004 (E), Comité Européen de Normalisation (CEN).

European-Mediterranean Seismological Centre (EMSC) (n.d.). Euro-Med Bulletin, available at https://www.emsc-csem.org/Bulletin/ (last accessed June 2021).

Fäh, D., F. Kind, and D. Giardini (2001). A theoretical investigation of average H/V ratios, *Geophys. J. Int.* **145,** no. 2, 535–549, doi: 10.1046/j.0956-540x.2001.01406.x.

Franceschina, G., S. Gentili, and G. Bressan (2013). Source parameters scaling of the 2004 Kobarid (Western Slovenia) seismic sequence, *Phys. Earth Planet. In.* **222,** 58–75, doi: 10.1016/j.pepi.2013.07.004.

Italian Seismological Instrumental and Parametric Data-Base (ISIDe) Working Group (2007). ISIDe: Italian Seismological Instrumental and Parametric Data-Base, available at http://terremoti.ingv.it/en/iside (last accessed June 2021).

Kawase, H., F. Nagashima, K. Nakano, and Y. Mori (2019). Direct evaluation of S-wave amplification factors from microtremor H/V ratios: Double empirical corrections to "Nakamura" method, *Soil Dynam. Earthq. Eng.* **126,** 105067, doi: 10.1016/j.soildyn.2018.01.049.

Klin, P., G. Laurenzano, and E. Priolo (2018). GITANES: A MATLAB package for estimation of site spectral amplification with the generalized inversion technique, *Seismol. Res. Lett.* **89,** no. 1, 182–190, doi: 10.1785/0220170080.

Klin, P., G. Laurenzano, M. A. Romano, E. Priolo, and L. Martelli (2019). ER3D: A structural and geophysical 3-D model of central Emilia-Romagna (northern Italy) for numerical simulation of earthquake ground motion, *Solid Earth* **10,** no. 3, 931–949, doi: 10.5194/se-10-931-2019.

Laurenzano, G., C. Barnaba, M. A. Romano, E. Priolo, M. Bertoni, P. L. Bragato, P. Comelli, I. Dreossi, and M. Garbin (2019). The Central Italy 2016–2017 seismic sequence: Site response analysis based on seismological data in the Arquata del Tronto–Montegallo municipalities, *Bull. Earthq. Eng.* **17,** no. 10, 5449–5469, doi: 10.1007/s10518-018-0355-3.

Laurenzano, G., E. Priolo, M. Mucciarelli, L. Martelli, and M. Romanelli (2017). Site response estimation at Mirandola by virtual reference station, *Bull. Earthq. Eng.* **15,** no. 6, 2393–2409, doi: 10.1007/s10518-016-0037-y.

Lermo, J., and F. J. Chávez-García (1993). Site effect evaluation using spectral ratios with only one station, *Bull. Seismol. Soc. Am.* **83,** no. 5, 1574–1594.

Malagnini, L., K. Mayeda, A. Akinci, and P. L. Bragato (2004). Estimating absolute site effects, *Bull. Seismol. Soc. Am.* **94,** no. 4, 1343–1352, doi: 10.1785/012003161.

Massa, M., C. Mascandola, C. Ladina, S. Lovati, and S. Barani (2017). Fieldwork on local-site seismic response in the Po Plain: Examples from ambient vibration array and single station analyses, *Bull. Earthq. Eng.* **15,** no. 6, 2349–2366, doi: 10.1007/s10518-016-0017-2.

Michel, C., B. Edwards, V. Poggi, J. Burjánek, D. Roten, C. Cauzzi, and D. Fäh (2014). Assessment of site effects in Alpine regions through systematic site characterization of seismic stations, *Bull. Seismol. Soc. Am.* **104,** no. 6, 2809–2826, doi: 10.1785/0120140097.

Moratto, L., M. A. Romano, G. Laurenzano, S. Colombelli, E. Priolo, A. Zollo, A. Saraò, and M. Picozzi (2019). Source parameter analysis of microearthquakes recorded around the underground gas storage in the Montello-Collalto Area (Southeastern Alps, Italy), *Tectonophysics* **762,** 159–168, doi: 10.1016/j.tecto.2019.04.030.

Nakamura, Y. (1989). A method for dynamic characteristics estimation of subsurface, *Q. Rep. Railway Tech. Res. Inst.* **30,** 25–33.

National Institute of Oceanography and Applied Geophysics (OGS) (n.d.). The Friuli-Venezia Giulia Seismometric Network Bulletin, available at http://www.crs.inogs.it/bollettino/RSFVG/RSFVG.en.html (last accessed February 2021).

Oth, A., D. Bindi, S. Parolai, and D. Di Giacomo (2011). Spectral analysis of K-NET and KiK-net data in Japan, part II: On attenuation characteristics, source spectra, and site response of borehole and surface stations, *Bull. Seismol. Soc. Am.* **101,** no. 2, 667–687, doi: 10.1785/0120100135.

Panzera, F., P. Bergamo, and D. Fäh (2020). Reference soil condition for intensity prediction equations derived from seismological and geophysical data at seismic stations, *J. Seismol.* **25,** doi: 10.1007/s10950-020-09962-z.

Parolai, S. (2012). Investigation of site response in urban areas by using earthquake data and seismic noise, *New Man. Seismol. Obs. Pract. 2 NMSOP-2*, 1–38, doi: 10.2312/GFZ.NMSOP-2_ch14.

Parolai, S., A. Ansal, A. Kurtulus, A. Strollo, R. Wang, and J. Zschau (2009). The Ataköy vertical array (Turkey): Insights into seismic wave propagation in the shallow-most crustal layers by waveform deconvolution, *Geophys. J. Int.* **178,** no. 3, 1649–1662, doi: 10.1111/j.1365-246X.2009.04257.x.

Parolai, S., D. Bindi, and P. Augliera (2000). Application of the generalized inversion technique (GIT) to a microzonation study: Numerical simulations and comparison with different site-estimation techniques, *Bull. Seismol. Soc. Am.* **90,** no. 2, 286–297, doi: 10.1785/0119990041.

Parolai, S., D. Bindi, M. Baumbach, H. Grosser, C. Milkereit, S. Karakisa, and S. Zünbül (2004). Comparison of different site response estimation techniques using aftershocks of the 1999 Izmit earthquake, *Bull. Seismol. Soc. Am.* **94,** no. 3, 1096–1108, doi: 10.1785/0120030086.

Picozzi, M., S. Parolai, and D. Albarello (2005). Statistical analysis of noise horizontal-to-vertical spectral ratios (HVSR), *Bull. Seismol. Soc. Am.* **95,** no. 5, 1779–1786, doi: 10.1785/0120040152.

Pilz, M., S. Parolai, F. Leyton, J. Campos, and J. Zschau (2009). A comparison of site response techniques using earthquake data and ambient seismic noise analysis in the large urban areas of Santiago de Chile, *Geophys. J. Int.* **178,** no. 2, 713–728, doi: 10.1111/j.1365-246X.2009.04195.x.

Pilz, M., S. Parolai, B. Petrovic, N. Silacheva, T. Abakanov, S. Orunbaev, and B. Moldobekov (2018). Basin-edge generated Rayleigh waves in the Almaty basin and corresponding consequences for ground motion amplification, *Geophys. J. Int.* **213,** no. 1, 301–316, doi: 10.1093/gji/ggx555.

Pischiutta, M., P. Cianfarra, F. Salvini, F. Cara, and P. Vannoli (2018). A systematic analysis of directional site effects at stations of the Italian seismic network to test the role of local topography, *Geophys. J. Int.* **214,** no. 1, 635–650, doi: 10.1093/gji/ggy133.

Poggi, V., C. Scaini, L. Moratto, G. Peressi, P. Comelli, P. L. Bragato, and S. Parolai (2021). Rapid damage scenario assessment for earthquake emergency management, *Seismol. Res. Lett.* doi: 10.1785/0220200245.

Priolo, E., C. Barnaba, P. Bernardi, G. Bernardis, P. L. Bragato, G. Bressan, M. Candido, E. Cazzador, P. Di Bartolomeo, G. Durì, *et al.* (2005). Seismic monitoring in Northeastern Italy: A ten-year experience, *Seismol. Res. Lett.* **76,** no. 4, 446–454, doi: 10.1785/gssrl.76.4.446.

Priolo, E., G. Laurenzano, C. Barnaba, P. Bernardi, L. Moratto, and A. Spinelli (2015). OASIS: The OGS Archive System of Instrumental Seismology, *Seismol. Res. Lett.* **86,** no. 3, 978–984, doi: 10.1785/0220140175.

Priolo, E., F. Pacor, D. Spallarossa, G. Milana, G. Laurenzano, M. A. Romano, C. Felicetta, S. Hailemikael, F. Cara, G. Di Giulio, *et al.* (2020). Seismological analyses of the seismic microzonation of 138 municipalities damaged by the 2016–2017 seismic sequence in Central Italy, *Bull. Earthq. Eng.* **18,** no. 12, 5553–5593, doi: 10.1007/s10518-019-00652-x.

Priolo, E., M. Romanelli, M. P. Plasencia Linares, M. Garbin, L. Peruzza, M. A. Romano, P. Marotta, P. Bernardi, L. Moratto, D. Zuliani, and P. Fabris (2014). Seismic monitoring of an underground natural gas storage facility: The Collalto Seismic Network, *Seismol. Res. Lett.* **86,** no. 1, 109–123, doi: 10.1785/0220140087.

Régnier, J., H. Cadet, L. F. Bonilla, E. Bertrand, and J. Semblat (2013). Assessing nonlinear behavior of soils in seismic site response: Statistical analysis on KiK-net strong-motion data, *Bull. Seismol. Soc. Am.* **103,** no. 3, 1750–1770, doi: 10.1785/0120120240.

Rovida, A., M. Locati, R. Camassi, B. Lolli, and P. Gasperini (2020). The Italian earthquake catalogue CPTI15, *Bull. Earthq. Eng.* **18,** no. 7, 2953–2984, doi: 10.1007/s10518-020-00818-y.

Sánchez-Sesma, F. J., M. Rodríguez, U. Iturrarán-Viveros, F. Luzón, M. Campillo, L. Margerin, A. García-Jerez, M. Suarez, M. A. Santoyo, and A. Rodríguez-Castellanos (2011). A theory for microtremor H/V spectral ratio: Application for a layered medium, *Geophys. J. Int.* **186,** no. 1, 221–225, doi: 10.1111/j.1365-246X.2011.05064.x.

Semblat, J. F., M. Kham, E. Parara, P. Y. Bard, K. Pitilakis, K. Makra, and D. Raptakis (2005). Seismic wave amplification: Basin geometry vs soil layering, *Soil Dynam. Earthq. Eng.* **25,** no. 7, 529–538, doi: 10.1016/j.soildyn.2004.11.003.

Spudich, P., W. B. Joyner, A. G. Lindh, D. M. Boore, B. M. Margaris, and J. B. Fletcher (1999). SEA99: A revised ground motion prediction relation for use in extensional tectonic regimes, *Bull. Seismol. Soc. Am.* **89,** no. 5, 1156–1170.

Stucchi, M., C. Meletti, V. Montaldo, H. Crowley, G. M. Calvi, and E. Boschi (2011). Seismic hazard assessment (2003–2009) for the Italian Building Code, *Bull. Seismol. Soc. Am.* **101,** no. 4, 1885–1911, doi: 10.1785/0120100130.

Tucker, B. E., J. L. King, D. Hatzfeld, and I. L. Nersesov (1984). Observations of hard-rock site effects, *Bull. Seismol. Soc. Am.* **74,** no. 1, 121–136.

Wald, D. J., V. Quitoriano, T. H. Heaton, H. Kanamori, C. W. Scrivner, and C. B. Worden (1999). TriNet "ShakeMaps": Rapid generation of peak ground motion and intensity maps for earthquakes in Southern California, *Earthq. Spectra* **15,** no. 3, 537–555, doi: 10.1193/1.1586057.

Zhu, C., M. Pilz, and F. Cotton (2020). Evaluation of a novel application of earthquake HVSR in site-specific amplification estimation, *Soil Dynam. Earthq. Eng.* **139,** 106301, doi: 10.1016/j.soildyn.2020.106301.